Contour into texture: information content of surface contours and texture flow

David C. Knill

University of Rochester, Center for Visual Sciences, 273 Meliora Hall, Box 270270, Rochester, New York 14627

Received October 14, 1999; revised manuscript received June 12, 2000; accepted June 26, 2000

Both surface contours and texture patterns can provide strong cues to the three-dimensional shape of a surface in space. Many of the most perceptually salient texture patterns have a strong flowlike structure, resulting from the directional nature of the surface textures from which they project. Under the minimal assumption that an oriented surface texture is homogeneous, the texture flow on a developable surface can be shown to follow parallel geodesics of the surface. The geometry of texture flow is therefore equivalent to that of an important class of surface contours: those that project from parallel geodesics of a developable surface. I derive a set of differential equations that support the estimation of surface shape from geodesic surface contours under spherical perspective, for both parallel and nonparallel contours. For perfectly oriented textures, the equations apply directly to the integrated flow lines in a texture image. For weakly oriented textures, perspective projection distorts the projected orientation of flow lines away from the idealized case of pure contours; however, simulations show that for a large class of textures, these distortions will be small and limited largely to extreme surface poses. The geometrical analysis, along with a number of phenomenal demonstrations and psychophysical results, suggests that the human visual system co-opts shape from contour mechanisms to estimate surface shape from texture flow.

OCIS codes: 330.4060, 330.5020, 150.0150.

1. INTRODUCTION

The projected images of surface markings provide strong cues to the shapes of surfaces, in the form of either contours or texture patterns (see Fig. 1). Researchers have generally categorized these cues into one of two classes, contours or texture, and have studied these cues within distinct computational and geometric frameworks. Homogeneous, oriented textures, however, flow over a surface in much the same way as contours; thus one might expect that the visual system would use a common mechanism for the recovery of shape from surface contours and shape from texture flow (see Figs. 2 and 3). I will show that the natural definition of homogeneity implies that oriented surface textures flow along parallel geodesics on developable surfaces; that is, the texture flows along curves that, when a developable surface is unfolded to be flat, are parallel and straight. Parallel geodesics on developable surfaces are also a natural class of surface markings, or edges. Straight lines on a ruled piece of paper are parallel geodesics of any surface formed by folding the paper. This paper analyzes the geometry of contours and texture flow lines that project from such curves and shows how they can be used to estimate surface shape.

The first part of the paper deals with the problem of estimating surface shape from contours that project from geodesics of developable surfaces (curves that unfold to straight lines when a developable surface is flattened). For generality, I will analyze the geometry of contours that project from nonparallel geodesics (e.g., the sides of a corner of a folded piece of paper) as well as parallel geodesics, though the latter is the special case that applies to texture flow. The first part of the paper (Sections 2 and 3) can be read as an independent contribution to solving the problem of estimating surface shape from surface contours. The second part of the paper (Sections 4 and 5) applies the results of the contour analysis to the problem of estimating surface shape from images of strongly oriented textures (texture flow) on developable surfaces. I will argue in the conclusion that because the visual system can "co-opt" contour mechanisms to infer shape from textures with significant, and detectable, oriented components, such textures may be more perceptually salient than other textures.

The paper is organized into five sections, including this introduction. The second section provides a review of previous shape-from-contour work. The third section analyzes the information provided by contours projected from geodesics on developable surfaces. This section takes a graded approach to the analysis, beginning with contours projected from parallel geodesics on developable surfaces under orthographic projection, followed by nonparallel geodesics (e.g., the corners of a folded page) under orthographic projection and finishing with the complete generalization to spherical perspective. In the fourth section, I show how the geometric analysis of Section 3 can be applied to the problem of inferring shape from texture flow. The final section describes evidence that texture flow is a particularly salient form of texture cue to surface shape and presents a number of demonstrations that support the contention that texture flow information is processed by contourlike mechanisms rather than by more generic texture gradient mechanisms. I also briefly discuss the problem of measuring texture flow in natural images.

2. PREVIOUS WORK ON SHAPE FROM SURFACE CONTOURS

Surface contours are contours in an image that project from extended markings on a surface. Surface markings

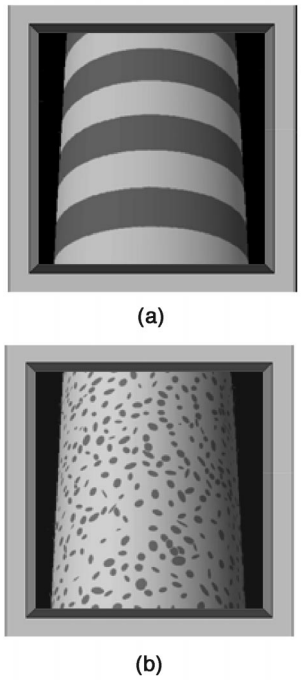

Fig. 1. Examples of surface markings that generate (a) image contours and (b) image texture. Both forms of information are strong cues to surface shape.

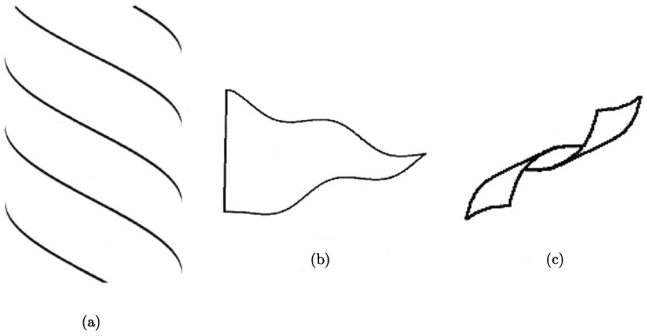

Fig. 2. Three examples of surface contours: (a) stripes on a circular cylinder that follow geodesics (but not lines of curvature), (b) pairs of geodesics that run in different directions on a cylindrical surface, and (c) the edges of a thin, developable surface that is folded and twisted in space. The contour pattern in (c) is not, technically, a surface contour but rather is a special kind of surface-orientation discontinuity, one formed by the edges of a thin surface. The pattern in (b) might also be formed from the edges of a thin surface such as a flag. The analysis presented in this paper applies to this class of contours as well as to surface contours. In fact, contours formed by the edges of thin surfaces are possibly the largest natural class of contours to which the analysis applies.

might, for example, correspond to the boundaries of material changes on a surface. Other types of contours exist in images that provide strong sources of information about surface shape. These include smooth occluding contours,[1,2] discontinuities in surface orientation,[3–7] and shadow boundaries.[8,9] The information underlying each of these types of contours has its own unique geometrical structure, which is generally different from the geometry of surface contours. The current analysis of contour information does, however, generalize to an important class of contours that are not projected from surface markings. These are contours projected from the edges of thin surfaces such as paper, sheets of metal, or blades of grass. Thin-surface edges may, in fact, be the largest class of contours to which our work applies; hence the reader should keep these in mind as candidate targets for the analysis.

Numerous computational models have been proposed to characterize the information content of surface markings. All of the models rely on assumptions about the geometry of the markings from which surface contours project to help constrain what are otherwise underdetermined problems. Types of surface markings covered by existing models include figures that are statistically isotropic (are drawn from a statistical ensemble of figures with, on average, no dominant orientation);[10–12] closed figures that are bilaterally symmetric;[13] parallel contours that follow lines of curvature on cylindrical surfaces;[14] geodesics on arbitrary, smooth surfaces and their equivalents on piecewise smooth surfaces;[15] and parallel, planar sections through linear, homogeneous, generalized cylinders (e.g., cones and cylinders).[16,17] Most of these categories of surface markings clearly represent natural kinds of markings, and thus have good ecological justification. Moreover, phenomenal demonstrations and in some cases the results of more rigorous psychophysical studies suggest that the visual system can, when appropriate, use each of the categories of surface contour constraints listed here.[11,14,15,18,19] The analysis presented in Section 3 extends the general model of contour information to include contours projected from geodesics on developable surfaces.

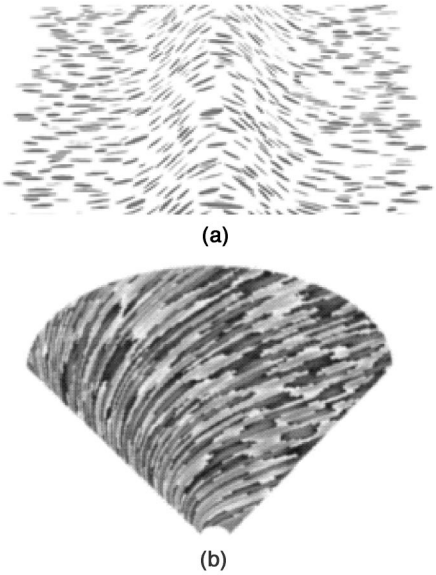

Fig. 3. Two examples of homogeneous, oriented textures on developable surfaces. These are created by isomorphically mapping (wrapping) planar textures onto developable surfaces: (a) a texture mapped onto a one-dimensional ridge in such a way that the texture "flows" along lines of curvature (a special case of geodesics), (b) a continuous texture mapped onto a cone. In this case, the texture "flows" along geodesics of the cone but not along the lines of curvature.

3. SHAPE FROM CONTOUR FOR CONTOURS PROJECTED FROM GEODESICS ON DEVELOPABLE SURFACES

Stevens[14] suggested that humans are predisposed to interpret smooth, extended surface contours as geodesics on a smooth surface. He analyzed a special case of geodesic contours: contours that project from lines of curvature on cylindrical surfaces. The current author[15] analyzed the information provided by surface contours under the more general assumption of geodesicity and found that, when surface shape was left unconstrained, the metric information provided by such contours was weak, although some qualitative shape information could be derived from the contours. Neither author was able to suggest a natural, synthetic model for surface markings on arbitrarily curved surfaces that would lead to a geodesic constraint.

Such a model does exist for a limited class of surfaces, namely, ones that are developable. Developable surfaces have zero Gaussian curvature everywhere; thus they can be mapped isometrically to a flat surface: they can be "unfolded," without stretching or compression, to a flat surface, unlike, for example, a sphere. Similarly, developable surfaces can be created by folding and twisting (without stretching or compressing) a flat surface. A natural class of markings on such surfaces are those that are straight on the flat surface before folding or would be straight should the surface be unfolded. The edges of a sheet of paper are prototypical cases in point. After being folded, the straight edges are twisted in three-dimensional (3D) space, with their curvature in space determined by the curvature of the underlying surface. One can easily show that surface markings created in this way are geodesics of the curved surface. Thus the local curvature of the markings is equal to the curvature of the underlying surface, in both direction and magnitude. Of course, processes other than folding can generate geodesic surface markings on a developable surface: for example, slicing a cylindrical surface perpendicular to its principal axis, threading a steel rod, or painting curves in a constrained way on developable surfaces.

Knowing that a contour is projected from a geodesic on a developable surface clearly provides significant constraint on the problem of estimating surface shape from contour. In this section I will show that the spherical image of two parallel geodesic curves on a developable surface is enough to uniquely determine the shape of the underlying surface. The analysis is built on the foundation of a basic relationship between local contour curvature and local surface curvature (derived in Ref. 15). We therefore begin with a brief review of geodesics and of this relationship.

A. Mathematical Notation

I will use the following mathematical conventions in the paper. Vector quantities defined in the image will be denoted by lowercase letters (e.g., $\mathbf{n}$ for the vector normal to a contour), and vector quantities defined in 3D space will be denoted by uppercase letters (e.g., $\mathbf{V}$ for viewing direction). Variables specifying surface properties will be denoted by the subscript S, as in $\mathbf{N}_S$, for the surface normal. Scalar variables will be lowercase. The following variables will appear prominently in the analysis:

- s arc length along a contour in the image
- s' arc length along a curve on a surface in space
- $\kappa(s)$ curvature of a contour expressed as a function of arc length along the contour
- $\kappa_g(s)$ geodesic curvature of a contour in a spherical image expressed as a function of arc length along the contour (the analog of planar curvature for planar images)
- $\kappa_{n_S}(s)$ normal curvature of the surface from which a contour projects expressed as a function of arc length along a contour in the image
- $\mathbf{t}(s)$ tangent to a contour expressed as a function of arc length along the contour
- $\mathbf{n}(s)$ normal to a contour expressed as a function of arc length along the contour
- $\mathbf{T}_S(s)$ tangent to the 3D curve that projects to a contour expressed as a function of arc length along the contour
- $\mathbf{N}_S(s)$ normal of the surface from which a contour projects expressed as a function of arc length along the contour
- $\mathbf{N}_S(s_{3D})$ normal of the surface from which a contour projects expressed as a function of arc length along the 3D curve on the surface that projects to the contour
- $\mathbf{V}$ viewing direction
- $\mathbf{V}(s)$ viewing direction to the curve that projects to a contour in the image expressed as a function of arc length along the contour (constant for orthographic projection, variable for spherical projection)
- $\mathbf{R}_S(s)$ unit-normal vector specifying the direction of surface rulings in space expressed as a function of arc length along a contour
- $\mathbf{r}(s)$ unit-normal vector specifying the projected direction of surface rulings in the image expressed as a function of arc length along a contour

Vectors defined in the image are assumed to be three dimensional; thus, for orthographic projection with a viewing direction along the z axis, vectors in the image plane have a z value of 0.

I will make use of two other mathematical conventions in the analysis. The notation $\langle \mathbf{x}, \mathbf{y} \rangle$ signifies the inner product between $\mathbf{x}$ and $\mathbf{y}$. The notation $\mathbf{x} \wedge \mathbf{y}$ signifies the outer product between $\mathbf{x}$ and $\mathbf{y}$.

B. Local Curvature Constraint for Geodesic Contours

In Ref. 15 I derived an expression relating the curvature of an image contour to the normal curvature of its underlying surface, under the assumption that the contour is projected from a geodesic of the surface under orthographic projection. I re-present the expression here, as it is fundamental to the solution of the shape-from-contour problem. The basic logic of the derivation is straightforward: the normal to a geodesic curve is equal to the surface normal, and its curvature is equal to the normal curvature of the surface; therefore the equation relating

contour curvature to 3D curvature in space also expresses the relationship between contour curvature and surface-normal curvature. Appendix A gives a derivation of the constraint for both orthographic and spherical perspective projections.

Proposition 1. Let γ be a contour in the image projected under orthographic projection from a geodesic curve, Γ, on a smooth surface (at least twice differentiable). With the notation defined in Subsection 3.B, the normal curvature of the surface in the tangent direction of Γ is given by

$$\kappa_{n_S}(s) = \frac{|[\mathbf{n}(s) \wedge \mathbf{N}_S(s)] \wedge \mathbf{V}(s)|\langle n(s) \wedge \mathbf{V}(s),\, n(s) \wedge \mathbf{N}_S(s)\rangle}{\langle \mathbf{N}_S(s) \wedge \mathbf{V}(s),\, n(s) \wedge \mathbf{V}(s)\rangle |\mathbf{n}(s) \wedge \mathbf{N}_S(s)|^2} \kappa(s); \quad (1)$$

where $\mathbf{V}$ is the viewing direction, usually taken to be $(0, 0, 1)^T$. A similar expression applies to contours generated from spherical projection.

Corollary. Let γ be a contour in the spherical image projected under spherical projection from a geodesic curve, Γ, on a smooth surface (at least twice differentiable). The normal curvature of the surface in the tangent direction of Γ is given by

$$\kappa_{n_S}(s) = \frac{1}{\rho(s)} \frac{|[\mathbf{n}(s) \wedge \mathbf{N}_S(s)] \wedge \mathbf{V}(s)|\langle \mathbf{n}(s) \wedge \mathbf{V}(s),\, \mathbf{n}(s) \wedge \mathbf{N}_S(s)\rangle}{\langle \mathbf{N}_S(s) \wedge \mathbf{V}(s),\, \mathbf{n}(s) \wedge \mathbf{V}(s)\rangle |\mathbf{n}(s) \wedge \mathbf{N}_S(s)|^2} \kappa_g(s), \quad (2)$$

where $\kappa_g(s)$ is the geodesic curvature of the contour on the view sphere (the spherical analog of planar curvature), $\mathbf{V}(s)$ is the viewing direction from a point along the image contour through the center of projection, and $\rho(s)$ is the distance from the center of projection to the corresponding point on the curve on the surface.

Equations (1) and (2) differ in two substantive ways. First, the viewing direction varies with position along a contour for spherical projection. Second, because of the scaling effect of perspective, the surface normal curvature at a point in the image is inversely related to the distance to the curve at that point.

Note on spherical versus planar perspective. We use spherical perspective in our analysis for two reasons. First, it is biologically appropriate. Second, the geometrical relationships for spherical perspective are considerably simpler than for planar perspective, as reflected in the near equivalence between Eqs. (1) and (2). This suggests that in applying the model to planar perspective images, one should first transform the planar perspective image into its spherical equivalent. This is easily done with the relation $\mathbf{x}_{\text{spher}} = \mathbf{x}_{\text{plan}}/|\mathbf{x}_{\text{plan}}|$.

Equations (1) and (2) imply a useful qualitative constraint relating the curvature of a geodesic contour in an image to the curvature of the underlying surface.

Definition: sign of curvature constraint. The surface underlying a contour projected from a geodesic curves in the same direction as the contour. By implication, planar points on developable-surfaces project to inflection points in geodesic contours.

Despite the usefulness of the qualitative constraint imposed on surface curvature, the shapes of contours projected from geodesics of generic surfaces clearly provide limited metric information about surface shape. Equation (1) constrains surface shape only along the contour, and weakly at that. One cannot, for example, use Eq. (1) to solve for the surface normals along the contour [the function $\mathbf{N}_S(s)$] without knowing something more about the surface. In Subsection 3.C I will show that using a pair of parallel geodesic contours projected from a developable surface, one can transform Eq. (1) into a differential equation for $\mathbf{N}_S(s)$. Solution of the differential equation provides an estimate of surface shape along the contours. For developable surfaces, this is enough to completely determine the shape of the surface between the contours.

C. Parallel Geodesics of Developable Surfaces: Orthographic Projection

Developable surfaces have two defining characteristics. First, they are ruled surfaces; that is, they are composed of connected sets of straight line segments, the rulings of the surface. Second, they have zero Gaussian curvature; that is, at every point on the surface, the first principal curvature of the surface, in the direction of a surface ruling, is zero. At any given point on a developable surface, therefore, the local shape is specified by the surface normal, the direction of the ruling at the point, and the second principal curvature. Furthermore, surface orientation (specified by the surface normal) remains constant along rulings of the surface; thus, knowing the surface normals along any curve on the surface fully specifies the shape of the surface along the rulings that intersect the curve. One can easily show that the surface normal function along a curve on a developable surface uniquely determines the directions of the rulings intersecting the curve;[20] thus the surface-normal function completely specifies the global shape of the surface, and the problem of estimating surface shape from a contour projected from that surface reduces to the problem of estimating the surface-normal function along the contour. (The surface normals of a developable surface along a curve on the surface specify the shape of the surface along rulings emanating from the curve. The rulings, however, may end in singularities of the surface, as on a crumpled piece of paper. Other rulings coming into a singular point (or line) may not intersect the geodesic in question; surface shape along such rulings would remain indeterminate.)

Recalling that the normal of a geodesic curve is equal to

the normal of the underlying surface, one can surmise from the above that any smooth curve in 3-space has associated with it a unique developable surface for which it is a geodesic (the surface whose normal function along the curve is equal to the normal function of the curve itself). A single contour, therefore, does not provide adequate constraint on the interpretation problem, even under the strong constraint that it is projected from a geodesic of a developable surface. Any 3D curve that could have projected to the contour admits its own unique interpretation as a geodesic of a developable surface. This ambiguity is greatly reduced by the projected image of a second geodesic on the surface. When the second geodesic is parallel to the first (in a generalized sense to be defined below), the lines of parallelism between the curves determine the directions of the projected surface rulings. These, in turn, greatly limit the family of admissable surface interpretations that match the geodesic constraint.

With the exception of cylindrical surfaces, developable surfaces do not admit curves that are strictly parallel in 3-space, that is, that are rigid translations of one another. Nevertheless, one can define a consistent notion of parallelism of curves on developable surfaces. In essence, parallel curves on a developable surface are ones that map to parallel curves in the plane when the surface is unfolded. This is stated more formally below (see also Fig. 4).

Definition. Two curves, Γ_1 and Γ_2, on a developable surface are parallel if the tangent field of Γ_1 maps to the tangent field of Γ_2 under parallel transport. In particular, if p_1 and p_2 are points on Γ_1 and Γ_2 connected by a surface ruling, the tangents of Γ_1 and Γ_2 at p_1 and p_2 are parallel [$\mathbf{T}_{\Gamma_1}(p_1) = \mathbf{T}_{\Gamma_2}(p_2)$].

Under orthographic projection, the tangent of a contour is a simple function of the tangent of the curve from which the contour projects, independent of position in the image. Since the tangents of two parallel curves on a developable surface are equal along rulings of the surface, they project to contours whose tangents are equal along the projected rulings of the surface. Thus contours projected from a pair of parallel curves on a developable surface have a generalized form of linear parallelism under orthographic projection: There exists a unique correspondence between points on the two contours such that the tangents of the contours at corresponding points are parallel. Furthermore, the lines of parallelism between the two contours are the projections of the rulings of the developable surface. Assuming that the surface has no singularities (points where the rulings intersect), the lines of parallelism between the two contours cannot intersect (see Fig. 4). Knowing that two contours project from parallel curves on a developable surface immediately provides a means for inferring the projected rulings of the surface. The projected rulings are themselves a strong source of qualitative information about the shape of the surface. They reflect the "twist" of the surface. When the projected rulings are parallel, the underlying surface is necessarily cylindrical.

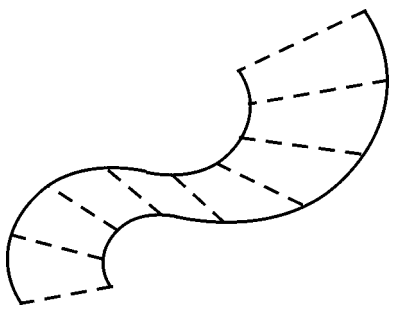

Fig. 4. Lines of parallelism between contours are the projections of surface rulings.

Knowledge of the projected rulings along a contour allows us to transform the equation for surface curvature, Eq. (1), into a first-order differential equation for $\mathbf{N}_S(s)$, the normal of the surface along the contour; that is, it allows us to derive an equation of the form

$$\frac{\partial \mathbf{N}_S(s)}{\partial s} = f(\mathbf{N}_S(s);\ \mathbf{r}(s),\ \mathbf{n}(s),\ \kappa(s),\ \mathbf{V}), \tag{3}$$

where $\mathbf{N}_S(s)$ is the normal of the surface along the contour, $\mathbf{r}(s)$ is a unit vector specifying the directions of the projected surface rulings in the image, $\mathbf{n}(s)$ is the normal to the contour, and $\kappa(s)$ is the curvature of the contour, all expressed as a function of arc length along the contour. $\mathbf{V}$ is a constant unit vector specifying the viewing direction. $\mathbf{r}(s)$, $\mathbf{n}(s)$, $\kappa(s)$, and $\mathbf{V}$ are given quantities [with $\mathbf{r}(s)$ inferred from the lines of parallelism between two contours]; thus they provide the data that parameterizes the differential equation. Integration of Eq. (3) determines the surface-normal function along the contour and hence the shape of the developable surface.

At the core of our derivation is a simple expression from differential geometry that specifies the rate of change of a surface's normal along a curve as a function of the normal curvature of the surface in the tangent direction of the curve,

$$\left|\frac{\partial \mathbf{N}_S(s')}{\partial s'}\right| = \left|\frac{\kappa_{n_S}(s')}{\sin[\theta(s')]}\right|, \tag{4}$$

where $\kappa_{n_S}(s')$ is the normal curvature of the surface, s' is arc length along the 3D curve on the surface, and θ is the angle between the tangent of the curve and the ruling of the surface. $\sin[\theta(s')]$ is given by

$$\sin[\theta(s')] = [1 - \langle \mathbf{R}_S(s'),\ \mathbf{T}_S(s')\rangle^2]^{1/2}. \tag{5}$$

where $\mathbf{R}_S(s')$ is a unit-normal vector function in the direction of surface rulings along the curve on the surface and $\mathbf{T}_S(s')$ is the tangent of the curve. Thus we have for the rate of change of the surface normal along a curve

$$\left|\frac{\partial \mathbf{N}_S(s')}{\partial s'}\right| = \left|\frac{\kappa_{n_S}(s')}{[1-\langle \mathbf{R}_S(s'),\ \mathbf{T}_S(s')\rangle^2]^{1/2}}\right|. \tag{6}$$

For a developable surface, the direction of surface orientation change given by $\partial \mathbf{N}_S(s')/\partial s'$ is perpendicular to the ruling. Since it is also perpendicular to $\mathbf{N}_S(s')$ (it lies in the tangent plane of the surface), we can express the

direction of $\partial \mathbf{N}_S(s')/\partial s'$ as a unit-normal vector given by the outer product of $\mathbf{R}_S(s')$ and $\mathbf{N}_S(s')$:

$$\frac{\partial \mathbf{N}_S(s')/\partial s'}{|\partial \mathbf{N}_S(s')/\partial s'|} = \begin{cases} [\mathbf{R}_S(s') \wedge \mathbf{N}_S(s')] : \kappa_{n_S}(s') \geq 0 \\ -[\mathbf{R}_S(s') \wedge \mathbf{N}_S(s')] : \kappa_{n_S}(s') < 0 \end{cases}; \tag{7}$$

thus $\partial \mathbf{N}_S(s')/\partial s'$ is given by

$$\frac{\partial \mathbf{N}_S(s')}{\partial s'} = \kappa_{n_S}(s') \frac{\mathbf{R}_S(s') \wedge \mathbf{N}_S(s')}{[1 - \langle \mathbf{R}_S(s'), \mathbf{T}_S(s') \rangle^2]^{1/2}}. \tag{8}$$

In order to convert Eq. (8) into a differential equation of the form given in Eq. (3), we need to express the 3D variables κ_{n_S}, $\mathbf{R}_S$, and $\mathbf{T}$ in terms of their equivalent image variables, κ, $\mathbf{r}$, and $\mathbf{n}$ (for compactness, we will use the contour normal in place of the tangent along the contour). We also need to reparameterize the equation in terms of arc length along the contour rather than arc length along the 3D curve on the surface. The latter is accomplished by postmultiplying with a correction factor, $\partial s'/\partial s$,

$$\frac{\partial \mathbf{N}_S(s)}{\partial s} = \kappa_{n_S}(s) \frac{\mathbf{R}_S(s) \wedge \mathbf{N}_S(s)}{[1 - \langle \mathbf{R}_S(s), \mathbf{T}_S(s) \rangle^2]^{1/2}} \frac{\partial s'}{\partial s}. \tag{9}$$

$\partial s'/\partial s$ is given by 1 over the cosine of the angle between the tangent to the contour and the tangent to the curve from which it projects,

$$\frac{\partial s'}{\partial s} = \frac{1}{\langle \mathbf{t}, \mathbf{T} \rangle}, \tag{10}$$

giving for $\partial \mathbf{N}_S(s)/\partial s$

$$\frac{\partial \mathbf{N}_S(s)}{\partial s} = \kappa_{n_S}(s) \frac{\mathbf{R}_S(s) \wedge \mathbf{N}_S(s)}{[1 - \langle \mathbf{R}_S(s), \mathbf{T}_S(s) \rangle^2]^{1/2}} \frac{1}{\langle \mathbf{t}(s), \mathbf{T}(s) \rangle}. \tag{11}$$

The unit-normal vector in the direction of the projected surface ruling, $\mathbf{r}$, can be backprojected onto the surface to obtain an expression for $\mathbf{R}_S$,

$$\mathbf{R}_S(s) = [\mathbf{r}(s) \wedge \mathbf{V}] \wedge \mathbf{N}_S(s) \frac{1}{|(\mathbf{r}(s) \wedge \mathbf{V}) \wedge \mathbf{N}_S(s)|}, \tag{12}$$

and similarly for $\mathbf{T}$,

$$\begin{aligned} \mathbf{T}_S(s) &= [\mathbf{t}(s) \wedge \mathbf{V}] \wedge \mathbf{N}_S(s) \frac{1}{|(\mathbf{t}(s) \wedge \mathbf{V}) \wedge \mathbf{N}_S(s)|}, \\ &= \mathbf{n}(s) \wedge \mathbf{N}_S(s) \frac{1}{|\mathbf{n}(s) \wedge \mathbf{N}_S(s)|}. \end{aligned} \tag{13}$$

Substituting Eqs. (12) and (14) for $\mathbf{R}_S(s)$ and $\mathbf{T}(s)$ and Eq. (1) for $\kappa_{n_S}(s)$ in equation (11) gives, finally,

$$\begin{aligned} \frac{\partial \mathbf{N}_S}{\partial s} = \kappa(s) & \frac{\{[\mathbf{r}(s) \wedge \mathbf{V}] \wedge \mathbf{N}_S(s)\} \wedge \mathbf{N}_S(s)}{|[\mathbf{r}(s) \wedge \mathbf{V}] \wedge \mathbf{N}_S(s)|} \\ & \times \frac{\|[\mathbf{n}(s) \wedge \mathbf{N}_S(s)] \wedge \mathbf{V}|}{\langle [\mathbf{N}_S(s) \wedge \mathbf{V}] \wedge \mathbf{V}, \mathbf{n}(s) \rangle |\mathbf{n}(s) \wedge \mathbf{N}_S(s)|} \\ & \times \frac{1}{\left\{1 - \left\langle \frac{[\mathbf{r}(s) \wedge \mathbf{V}] \wedge \mathbf{N}_S(s)}{|[\mathbf{r}(s) \wedge \mathbf{V}] \wedge \mathbf{N}(s)|}, \frac{\mathbf{n}(s) \wedge \mathbf{N}_S(s)}{|\mathbf{n}(s) \wedge \mathbf{N}_S(s)|} \right\rangle^2 \right\}^{1/2}}. \end{aligned} \tag{14}$$

Equation (14) is a first-order, nonlinear differential equation; thus we need only specify boundary conditions to solve for $\mathbf{N}_S(s)$ and derive an estimate of surface shape. The information provided by a pair of parallel geodesic contours can therefore be said to determine the underlying surface shape to within two degrees of freedom. A convenient way to think of the degrees of freedom is that they specify the global orientation of the surface. Stevens's [14] model of contour interpretation is a special case of the current formulation, in which the geodesics are assumed to follow lines of curvature on a surface. In our context, the line-of-curvature assumption can be thought of as adding one more constraint on the interpretation, reducing the degrees of freedom in the estimation problem to one (which Stevens resolved by selecting a minimum-slant solution).

D. Validating the Parallel-Geodesics Assumption

The previous analysis is useful only to the extent that one can rely on the assumption that a pair of contours in an image projects from parallel geodesics on a developable surface. The problem of determining the validity of an assumption for a particular set of image data is widespread in vision. One solution to the problem is to rely on "key features" in an image to infer reliably which of several candidate models should apply to the data in the image.[21] Key features are those that appear in images of one category of objects (or scenes) but are highly unlikely to appear in images of others. Skew symmetry in an image, for example, is a key feature for planar, bilateral symmetry in the world (under orthographic projection). This is because planar, bilateral symmetries always project to skew symmetries in the image, whereas asymmetric figures almost never do, except, possibly, in accidental views of an asymmetric figure.

The logical candidate for a key feature for the "parallel geodesics on a developable surface" constraint is the generalized form of linear parallelism that all projections of such curves display. In order to serve as a key feature, linear parallelism should not, in general, appear as a result of projecting other types of curves into the image. For unrelated pairs of curves on a surface, this is certainly the case: The probability of any two such curves projecting to contours with general linear parallelism is zero. There exist, however, at least two natural categories of curves that project to special cases of linearly parallel contours: Lines of curvature on cylindrical surfaces project to strictly parallel contours under orthographic projection,[14] and parallel, planar sections made perpendicular to the axes of linear generalized homogeneous cylinders project to contours related by a simple translation and scaling[17] (see Fig. 5 for examples). The former is a special case of parallel geodesics. The latter, however, is a distinct category. Thus we have the following logical implicatures (based on a general position argument):

A. Strict parallelism ⇒ Parallel geodesics on a cylindrical surface (which may be lines of curvature)

B. Scaled parallelism ⇒ Parallel geodesics on a developable surface *or* Planar sections perpen-

dicular to the axes of a linear generalized homogeneous cylinder

C. Linear parallelism ⇒ Parallel geodesics on a noncylindrical developable surface and not (A or B)

Except for the special case of scaled parallelism, linear parallelism reliably implicates the parallel-geodesics constraint under orthographic projection. In real imaging situations, however, measurement noise and perspective effects create some difficulties in reliably detecting contour parallelism. Thus ancillary information in the image may generally be needed to validate the constraint. Examples include the shapes of self-occluding contours and of shading isophotes on a surface. When these shapes are straight, they determine that the underlying surface is developable (for shading, this applies to Lambertian surfaces or away from specular highlights). They also determine the directions of local surface rulings.

E. Nonparallel Geodesics on Developable Surfaces

Contours projected from parallel geodesics on developable surfaces afford particularly straightforward computations for the derivation of 3D surface shape; however, parallelism is a fairly restrictive limitation on the scope of the analysis. In this section we deal with the problem of estimating surface shape from contours projected from nonparallel geodesics on developable surfaces. These are curves that map to straight but nonparallel lines when a surface is unfolded. Figure 2(b), of a triangular flag flapping in the wind, shows a prototypical example of such a set of contours.

Nonparallel geodesic contours contain no simple feature such as lines of parallelism to determine the projected surface rulings. This means that one cannot decompose the shape-interpretation process into two stages:

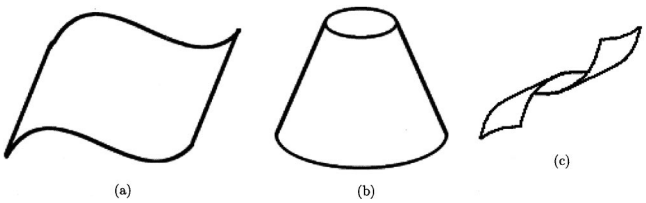

Fig. 5. Examples of the three different types of parallel contours discussed in the text: (a) strictly parallel contours, (b) scaled parallel contours (the top and bottom elliptical arcs), and (c) general linear parallel contours.

first estimating the projected surface rulings, then using those to help solve the surface-normal-constraint equation to estimate surface shape. Rather, one must estimate the projected rulings simultaneously with the surface-normal function along one of the contours. The greater computational complexity of the problem is offset by what we will see to be the increased information provided by having images of two nonparallel geodesics on a surface.

A specification of the projected ruling vector $\mathbf{r}_1(s)$ along one contour defines a continuous mapping between points on that contour and points on the second contour. We can express this as a function that maps arc length along the first contour to arc length along the second contour,

$$\mathbf{r} : s_1 \rightarrow s_2 \; ; \; s_2 = f(s_1, \mathbf{r}(s_1)), \tag{15}$$

where $f(s_1, \mathbf{r}(s_1))$ is the function mapping arc length along one contour to arc length along the other contour along surface rulings. At each point along the first contour, then, we have two constraints, one induced by the curvature and orientation of the first contour and the other induced by the curvature and orientation of the second contour,

$$\frac{\partial \mathbf{N}_S}{\partial s_1} = \kappa_1(s_1) \frac{\{[\mathbf{r}(s_1) \wedge \mathbf{V}] \wedge \mathbf{N}_S(s_1)\} \wedge \mathbf{N}_S(s_1)}{|[\mathbf{r}(s_1) \wedge \mathbf{V}] \wedge \mathbf{N}_S(s_1)|} \frac{|[\mathbf{n}_1(s_1) \wedge \mathbf{N}_S(s_1)] \wedge \mathbf{V}|}{\langle [\mathbf{N}_S(s_1) \wedge \mathbf{V}] \wedge \mathbf{V}, \mathbf{n}_1(s_1) \rangle |\mathbf{n}_1(s_1) \wedge \mathbf{N}_S(s_1)|} \times \frac{1}{\left\{ 1 - \left\langle \frac{[\mathbf{r}(s_1) \wedge \mathbf{V}] \wedge \mathbf{N}_S(s_1)}{|[\mathbf{r}(s_1) \wedge \mathbf{V}] \wedge \mathbf{N}_S(s_1)|}, \frac{\mathbf{n}_1(s_1) \wedge \mathbf{N}_S(s_1)}{|\mathbf{n}_1(s_1) \wedge \mathbf{N}_S(s_1)|} \right\rangle^2 \right\}^{1/2}}. \tag{16}$$

$$\frac{\partial \mathbf{N}_S}{\partial s_2} = \kappa_2(s_2) \frac{\{[\mathbf{r}(s_2) \wedge \mathbf{V}] \wedge \mathbf{N}_S(s_2)\} \wedge \mathbf{N}_S(s_2)}{|[\mathbf{r}(s_2) \wedge \mathbf{V}] \wedge \mathbf{N}_S(s_2)|} \frac{|[\mathbf{n}_2(s_2) \wedge \mathbf{N}_S(s_2)] \wedge \mathbf{V}|}{\langle [\mathbf{N}_S(s_2) \wedge \mathbf{V}] \wedge \mathbf{V}, \mathbf{n}_2(s_2) \rangle |\mathbf{n}_2(s_2) \wedge \mathbf{N}_S(s_2)|} \times \frac{1}{\left\{ 1 - \left\langle \frac{[\mathbf{r}(s_2) \wedge \mathbf{V}] \wedge \mathbf{N}_S(s_2)}{|[\mathbf{r}(s_2) \wedge \mathbf{V}] \wedge \mathbf{N}_S(s_2)|}, \frac{\mathbf{n}_2(s_2) \wedge \mathbf{N}_S(s_2)}{|\mathbf{n}_2(s_2) \wedge \mathbf{N}_S(s_2)|} \right\rangle^2 \right\}^{1/2}}, \tag{17}$$

where s_1 is arc length along one contour and s_2 is arc length along the other, $s_2 = f(s_1, \mathbf{r}(s_1))$. Given the implicit mapping between s_1 and s_2 determined by the surface rulings, we have, by definition, $\mathbf{r}(s_1) = \mathbf{r}(f(s_1, \mathbf{r}(s_1)))$ and $\mathbf{N}_S(s_1) = \mathbf{N}_S(f(s_1, \mathbf{r}(s_1)))$, and we can reparameterize the second constraint [Eq. (17)] as a function of arc length along the first contour, s_1, giving

$$\frac{\partial \mathbf{N}_S}{\partial s_1} = \kappa_2(s_1)\frac{\{[\mathbf{r}(s_1)\wedge\mathbf{V}]\wedge\mathbf{N}_S(s_1)\}\wedge\mathbf{N}_S(s_1)}{|[\mathbf{r}(s_1)\wedge\mathbf{V}]\wedge\mathbf{N}_S(s_1)|}\frac{|[\mathbf{n}_2(s_1)\wedge\mathbf{N}_S(s_1)]\wedge\mathbf{V}|}{\langle[\mathbf{N}_S(s_1)\wedge\mathbf{V}]\wedge\mathbf{V},\,\mathbf{n}_2(s_1)\rangle|\mathbf{n}_2(s_1)\wedge\mathbf{N}_S(s_1)|}$$
$$\times\frac{1}{\left\{1-\left\langle\frac{[\mathbf{r}(s_1)\wedge\mathbf{V}]\wedge\mathbf{N}_S(s_1)}{|[\mathbf{r}(s_1)\wedge\mathbf{V}]\wedge\mathbf{N}_S(s_1)|},\frac{\mathbf{n}_2(s_1)\wedge\mathbf{N}_S(s_1)}{|\mathbf{n}_2(s_1)\wedge\mathbf{N}_S(s_1)|}\right\rangle^2\right\}^{1/2}}\frac{\partial s_2}{\partial s_1}, \quad (18)$$

where $\partial s_2/\partial s_1$ is the derivative of the function mapping s_1 to s_2. Together with Eq. (16), this gives an overdetermined pair of differential equations in $\mathbf{N}_S(s_1)$, coupled by the function $\mathbf{r}(s_1)$.

The projected surface ruling function, $\mathbf{r}(s_1)$, is *a priori* unknown and must be solved simultaneously with the surface normal function $\mathbf{N}_S(s_1)$. The pair of differential equations, therefore, specifies four constraints in three unknowns: two for the surface normal function itself and one for the function $\mathbf{r}(s_1)$ (a unit-normal function in two dimensions). This leads to the conjecture that a pair of contours projected from nonparallel geodesics on a developable surface actually overdetermines the shape of the surface. Thus images of pairs of nonparallel geodesics on a developable surface should be more informative than images of parallel geodesics.

The difficulty in estimating surface shape from nonparallel geodesic contours lies in the complexity of the computations involved in solving for the projected surface rulings in parallel with the surface-normal function. This requires a nonlinear, nonlocal search process. Such a process would be greatly aided by good initial approximations of the surface rulings. Two ways to do this immediately present themselves. The first is based on the observation that inflections in the surface necessarily give rise to inflections in the projected contours. Thus, connecting inflection points in a pair of contours and interpolating the remaining surface rulings between them should provide a good initial approximation of the projected rulings. A second method is to use occluding contours or shading information to constrain the estimate of projected rulings. Developable surfaces with matte reflectance have the property that isophotes of the shading pattern (curves of equal luminance) follow the rulings of the surfaces; thus the isophotes of a shading pattern (away from specularities) can potentially provide reliable information about the directions of projected surface rulings.

F. Generalization to Spherical Perspective

Orthographic projection is clearly an approximation that holds only for small fields of view and for surfaces that are near to frontoparallel. This section generalizes the analysis to the more natural model of spherical perspective. The principal problem with perspective projection is that even when a pair of contours projects from parallel geodesics, the contours do not exhibit any form of parallelism in the image, and one cannot directly infer the projections of the surface rulings from the contours. This problem can be dealt with in the same way as the problem of nonparallel geodesics, that is, by setting up an overdetermined pair of differential equations in the surface-normal function along one of a set of contours and simultaneously solving for the projected rulings and the surface-normal function along the contour.

Under spherical projection, points in the world are projected through a nodal point at the center of a unit sphere to points on the sphere (called the view sphere). The view sphere is the geometric analog of the mammalian retina. We represent the position of a projected point on the view sphere as a unit-length vector in the direction of the ray that connects the surface point to the nodal point of the projection. In this characterization, the position of a point on the view sphere is simply the negative of the viewing direction from the eye (or camera) to the corresponding point in the world.

The curvature of a contour formed by spherical projection is given by its geodesic curvature on the view sphere. For example, a straight line in the world projects to a great circle on the view sphere, which, being a geodesic of the view sphere, has zero geodesic curvature. The corollary to proposition 1 states that the equation that relates contour curvature to surface curvature for spherical projection is equivalent to the one derived for orthographic projection, with a depth scaling factor added to compensate for perspective scaling effects. Thus the derivation of a differential equation for $\partial N/\partial s$ is qualitatively the same as the derivation for orthographic projection. In fact, because the term, $\partial s'/\partial s$ scales linearly with distance, $\rho(s)$, the distance term drops out of the differential equation, and we are left with an equation equivalent in form to that derived for orthographic projection. Thus we have for $\partial \mathbf{N}_S/\partial s$,

$$\frac{\partial \mathbf{N}_S(s)}{\partial_S} = \kappa_g(s)\frac{\{[\mathbf{r}(s)\wedge\mathbf{V}(s)]\wedge\mathbf{N}_S(s)\}\wedge\mathbf{N}_S(s)}{|[\mathbf{r}(s)\wedge\mathbf{V}(s)]\wedge\mathbf{N}_S(s)|}\frac{|[\mathbf{n}(s)\wedge\mathbf{N}_S(s)]\wedge\mathbf{V}(s)|}{\langle[\mathbf{N}_S(s)\wedge\mathbf{V}(s)]\wedge\mathbf{V}(s),\,\mathbf{n}(s)\rangle|\mathbf{n}(s)\wedge\mathbf{N}_S(s)|}$$
$$\times\frac{1}{\left\{1-\left\langle\frac{[\mathbf{r}(s)\wedge\mathbf{V}(s)]\wedge\mathbf{N}_S(s)}{|[\mathbf{r}(s)\wedge\mathbf{V}(s)]\wedge\mathbf{N}_S(s)|},\frac{\mathbf{n}(s)\wedge\mathbf{N}_S(s)}{|\mathbf{n}(s)\wedge\mathbf{N}_S(s)|}\right\rangle^2\right\}^{1/2}}. \quad (19)$$

The only difference between Eqs. (19) and (14) are that the planar image curvature term, $\kappa(s)$, has been replaced by the geodesic curvature of a contour on the view sphere, $\kappa_g(s)$, and the constant view vector $\mathbf{V}$ has been replaced by a vector function that varies with position along the contour $\mathbf{V}(s)$.

Because parallel contours projected onto the view sphere do not support direct estimation of the projected rulings, solving for surface shape along a contour on the view sphere should follow the same procedure as for contours projected from nonparallel geodesics under orthographic projection. The only difference is that the function specifying the directions of projected rulings, $\mathbf{r}(s)$, expresses orientation in the tangent plane of the view sphere. The function mapping points on two contours that share the same ruling is given by tracing great circles in the direction of $\mathbf{r}(s)$ away from points along one of the contours until they intersect the other contour. The two differential equations derived from a pair of contours in a spherical image are equivalent in form to those in Eqs. (18), with the planar curvature terms, κ_1 and κ_2, replaced by geodesic curvature terms, κ_{g1} and κ_{g2}.

Under orthographic projection, the absolute depth of the surface is indeterminate. Similarly, for perspective projection, the depth is indeterminate, and the absolute scale (size) of the estimated surface covaries with the estimated distance of the surface.

G. Simulations

I performed a number of simulations designed to validate the geodesic-constraint equations presented in Eqs. (14) and (19) and to explore the ambiguity in the information provided by images of parallel geodesic contours. Since orthography provides a reasonably good approximation to perspective projection for small fields of view and for surfaces with low slants away from the frontoparallel, the ambiguities inherent under orthographic projection reflect the uncertainty imposed by noise for a wide range of perspective images as well. The first set of simulations presented here, therefore, explores the nature of the ambiguity in the information provided by orthographic projections of parallel geodesic contours. The final simulation illustrates the solution of the shape-from-contour problem for perspective projection.

For the simulations, I used idealized representations of contours, unperturbed by noise or quantization errors. The first two simulations took as input synthetic pairs of parallel curves in the image [e.g., Fig. 6(a)]. The curves were generated in the image plane and not as projections from geodesics on prespecified surfaces. The direction of surface rul1ings (vertical) was specified for the simulations. I solved the geodesic-constraint equation in the simplest manner possible, using discrete differences to compute contour curvature and a Euler method to numerically integrate the equation.

Under orthographic projection, the ambiguity in surface interpretation lies in the initial conditions for the solution of the differential equation. Rather than choose random initial values for the surface normal, we set the initial conditions by selecting, for an initial point along a contour, the slant σ of the surface ruling at that point (its orientation out of the frontoparallel plane) and the angle θ between the geodesic curve on the surface and the surface ruling. These two values, along with the tangent direction of the curvature at the initial point, determine the initial surface orientation.

The stimuli for the first simulation were a pair of elliptical arcs [Fig. 6(a)]. In this simulation, the angle made by the inferred curves and the surface rulings was fixed at 90°; that is, the curves were assumed to follow lines of curvature on the surface. Figures 6(b), 6(c), and 6(d) show the surfaces estimated for three different slants. The notable property of the solutions is that the surface curvature decreases with increasing slant. This follows from the fact that for a fixed surface shape, contour curvature would increase with global surface slant. Perceptually, we appear to prefer the most regular solution: the circular cylinder.

The stimuli for the second simulation were a pair of sinusoidal segments [Fig. 7(a)]. In this simulation I fixed the slant of the surface rulings and varied the assumed orientation between the curve on the surface and the surface rulings. Figures 7(b) and 7(c) show the surfaces estimated assuming that the curves on the surface made angles of 90° and 75° with the surface rulings. The surface interpretations are dramatically different, although we clearly prefer the line-of-curvature interpretation. Figure 7(d) illustrates the difference more dramatically. In this figure I have projected the lines of curvature of both surfaces into the image from the same viewing position used in the simulation.

The two simulations clearly demonstrate the ambiguity in the interpretation of surface shape from pairs of orthographically projected, parallel, geodesic curves. They also demonstrate the two prior constraints that the human visual system uses to disambiguate the interpretation: a line-of-curvature constraint on the direction of curves on surfaces and a regularity (smoothness, symmetry) constraint on the shapes of surfaces.

As noted in Subsection 3.F, images of nonparallel geodesics disambiguate the surface interpretation. Figure 8 illustrates this by showing one of the pair of sine-wave contours used in simulation 2, paired with another, nonparallel, contour generated from each of three different surface interpretations consistent with the shape of the sine-wave contour (corresponding to $\theta \in \{90°, 80°, 70°\}$). The addition of the nonparallel geodesic contours clearly disambiguates the shapes of the surfaces, as reflected in the differing percepts of surface shape elicited by the three images.

The final simulation demonstrates the solution method for perspective projection. Figure 9(a) shows a pair of contours projected from lines of curvature on a sinusoidal surface viewed under perspective projection so that the image subtended 32° by 45° of visual angle. The pair of constraint equations defined by each contour was solved assuming knowledge that the rulings were vertical in the image. A unique solution for the surface shape was found by searching for the combination of σ and θ that minimized the difference between the surface-normal functions derived for each contour. This correctly gave a surface with a 0° slant and with curves following lines of curvature on the surface ($\theta = 90°$). Figure 9(b) shows a 3D plot of the derived surface, which was equivalent, with

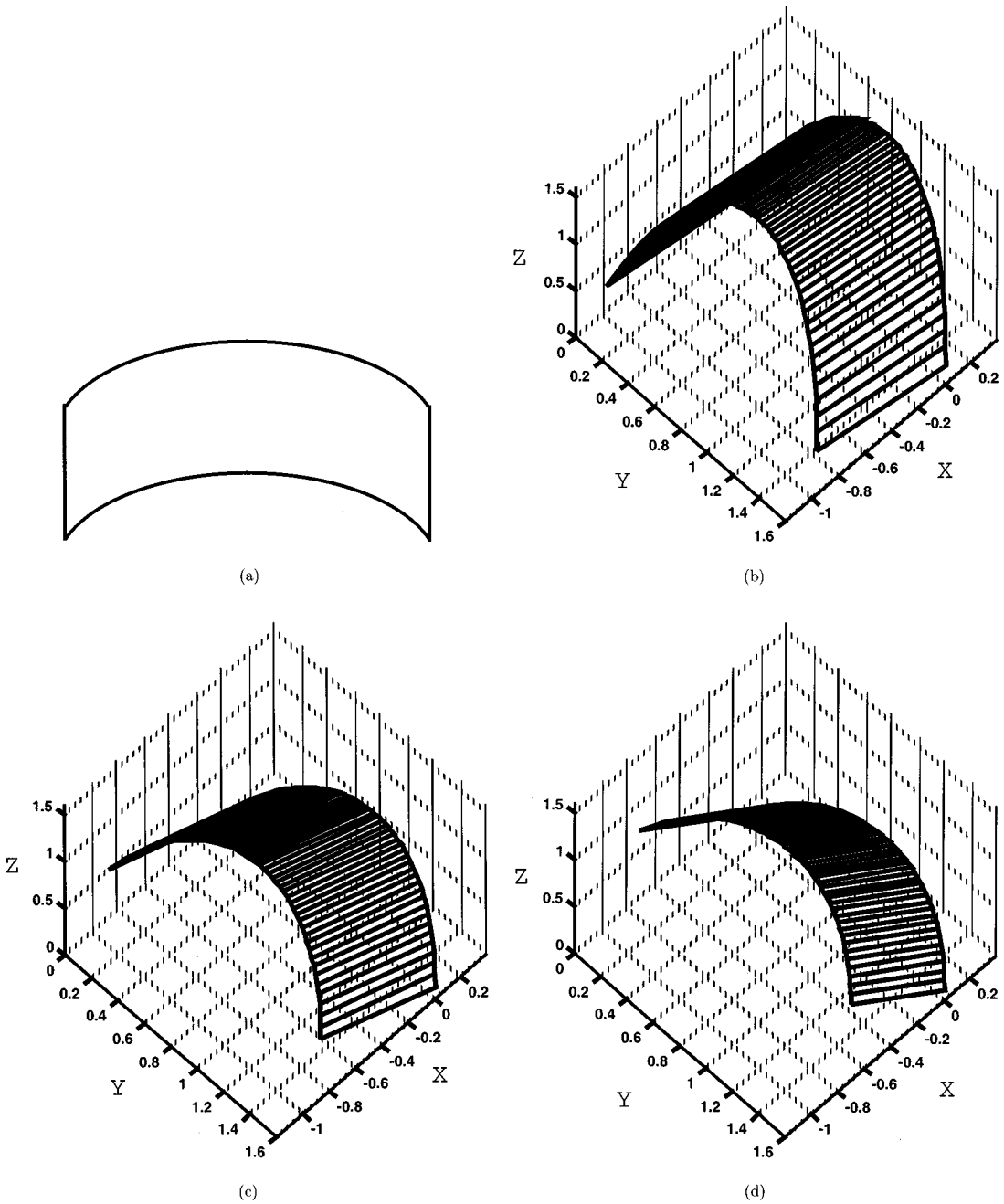

Fig. 6. (a) Parallel set of elliptical arcs, as might be projected from a segment of a circular cylinder slanted away from the front parallel by 30°. (b), (c), (d) Reconstructions of the surface shape from the contours in (a) for three different assumed surface slants: 15°, 30°, and 45°, respectively. Line of sight was along the z axis.

small numerical errors, to the original surface used to generate the contours. The method was further corroborated with a large number of other surfaces and viewing angles.

The simulations shown here take as input idealized representations of contours and do not deal with a number of preprocessing problems that must be solved for practical application of the model. Implementation of a system for solving shape from contour requires that contours be extracted from images, that they be accurately labeled (i.e., as surface markings versus smooth occluding contours), and that they be paired together for solution of the geodesic-constraint equations. Each of these problems is a difficult one to solve in its own right and is beyond the scope of this paper. I would like to note, however, one implementation issue that arises from the discrete and noisy nature of any putative contour representation. Because of the use of first- and second-derivative information in the geodesic-constraint equations, one will necessarily have to regularize the contour representation (e.g., by fitting splines to the contour data) to support a stable numerical solution of the geodesic-constraint equations. This will also allow subsampling of the contours for the numerical integration. Because of the qualitative similarity between the shapes of surfaces inferred from geodesic contours and the shapes of the con-

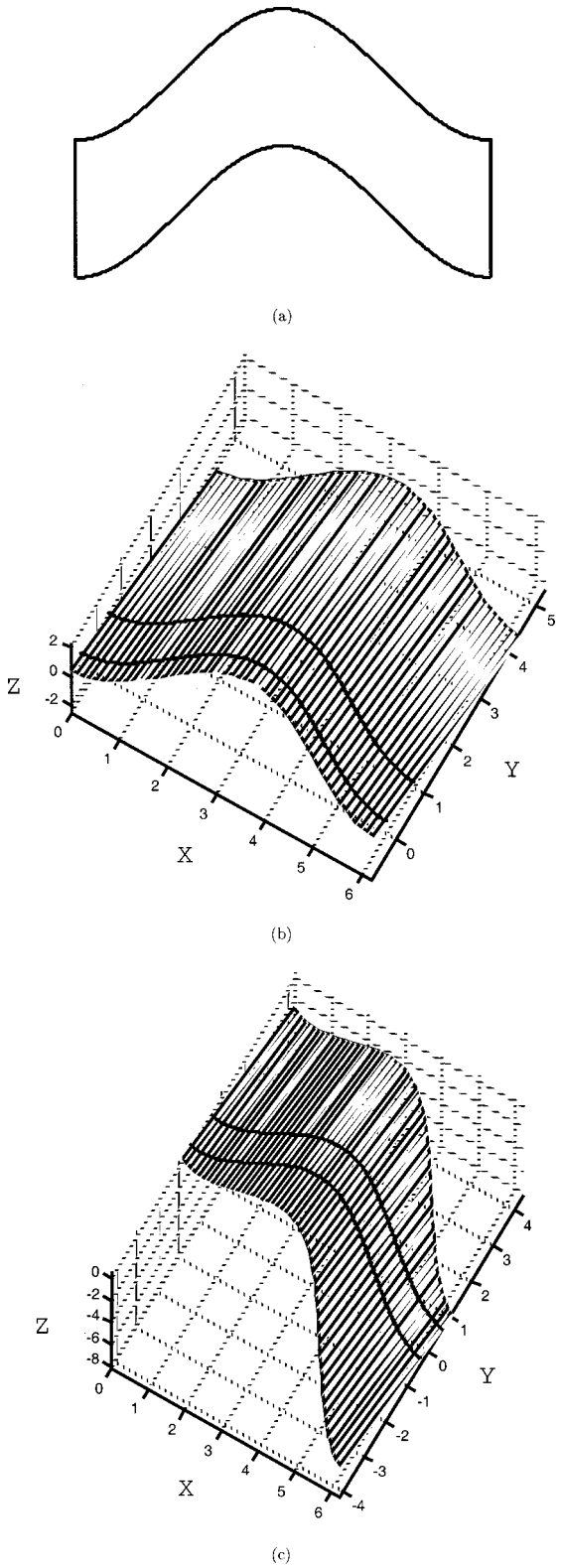

Fig. 7. (a) Parallel set of sinusoidal arcs. (b), (c) Reconstructions of the surface shape from the contours in (a) for two different assumed orientations of the surface markings on the surface relative to the surface rulings; (b) shows the surface reconstructed for an assumed marking orientation of 90° (a line of maximal curvature on the surface); (c) shows the surface reconstructed for an assumed marking orientation of 70°. The global surface orientation was assumed to be 30°. Line of sight was along the z axis. The solid curved lines in (b) and (c) indicate the backprojections of the surface markings shown in (a).

tours themselves, the errors in shape interpretation induced by contour measurement noise will be qualitatively similar to the errors in contour shape estimation.

H. Summary of Main Results

I have characterized the information provided by images of geodesic curves on developable surfaces. The case of parallel curves under orthorgraphic projection is the simplest. In this case, the projected surface rulings are given by the lines of parallelism between two contours. The direction of the projected surface rulings along one of the contours and the shape characteristics of the contour together parameterize a nonlinear first-order differential equation for the surface-normal function (the vector function specifying the surface normals along a contour). Since surface orientation is constant along rulings of a developable surface, this function effectively specifies the shape of the underlying surface. The geodesic-constraint equation leaves only two degrees of freedom undetermined, corresponding to the initial conditions for solution of the equation. Applying Stevens's assumption that sur-

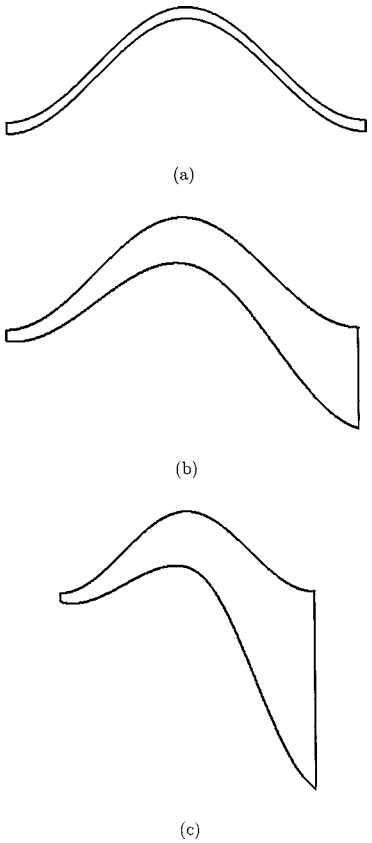

Fig. 8. The pair of contours in (a) ambiguously determine the shape of the underlying surface (under orthographic projection). Humans appear to resolve this ambiguity in part by assuming that the surface markings follow lines of curvature on a surface. (b), (c) Pairs of nonparallel geodesic contours uniquely determine the underlying surface shape. In these figures the upper contour has the same shape as the curves in (a). The second geodesic contour, however, disambiguates the shape, and we see the figures as all having different shapes, corresponding to cases in which the sinusoidal contour does not follow a line of surface curvature.

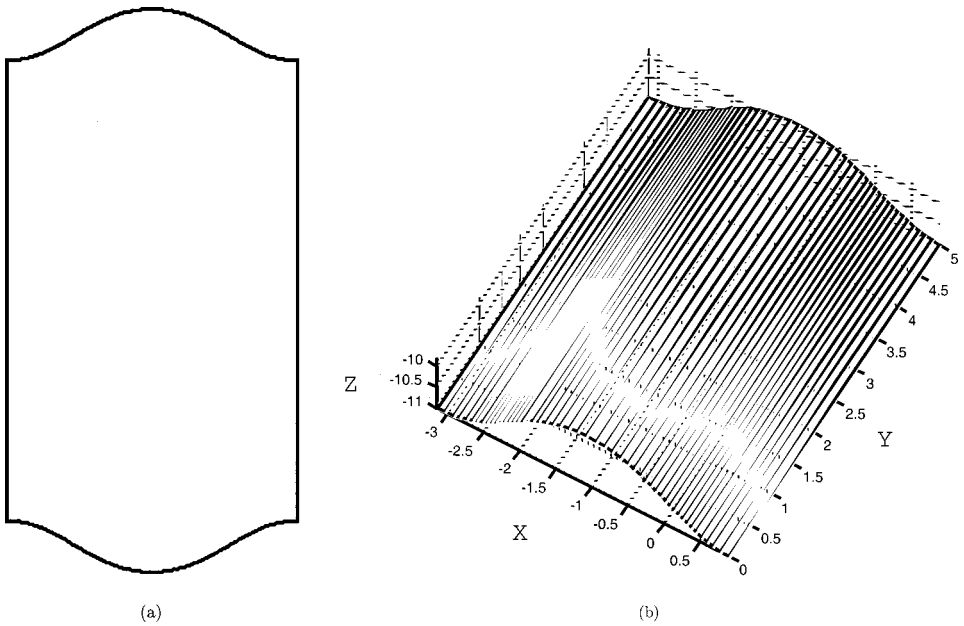

(a) (b)

Fig. 9. (a) Perspective projections of a pair of parallel geodesics on a sinuoidal surface viewed from above. (b) The surface was reconstructed by assuming that the ruling directions were fixed in the image at vertical (in this case, specified by the boundaries). The global orientation of the surface (0° out of the frontoparallel plane) and of the surface markings (90° form the rulings, i.e., lines of curvature) were correctly estimated from the image, as described in the text. Perspective projection supports the unambiguous estimation of surface shape.

face markings follow lines of curvature of the surface removes one degree of freedom but can be applied only to cylindrical surfaces.

The analysis can be generalized to arbitrary (i.e., not necessarily parallel) geodesic curves viewed under spherical perspective. Under perspective projection, however, the geometry of the contours does not directly determine the projected surface rulings. For a fixed set of projected surface rulings, the contours specify two independent first-order differential equations for the surface-normal function along one of the contours. One must solve these equations simultaneously with the estimation of the surface rulings to compute the surface normal function. The fact that the equations locally define four constraints on three unknowns (the surface normal and the projected ruling direction) leads to the conjecture that they overdetermine the surface shape, in which case perspective projections of geodesic surface markings provide more information than do orthographic projections of parallel markings. It should be noted that orthographic projection is a reasonable approximation to perspective for small fields of view, suggesting that perspective effects will often not contribute significantly to the informativeness of a pair of surface contours. It remains true, however, that contours that project from nonparallel markings are more informative than contours that project from parallel surface markings. This increase in informativeness comes at the cost of added computational complexity required to solve the constraint equations.

4. CONTOUR INTO TEXTURE

Figure 3 shows a texture pattern that elicits a strong perception of surface curvature. The texture shown in the figure is best described as a "texture flow," as it appears to be well characterized by the two-dimensional (2D) vector field of local texture orientations. A natural approach to estimating surface shape from texture flow would be to treat it in the same way as shape from contour; that is, the information contained in texture flow, because it is carried by the orientation field, is analagous to the information contained in extended surface contours. In this section I show that homogeneous, oriented textures on developable surfaces have the same geometric structure as the surface contours analyzed earlier in this paper: The average texture flow lines follow parallel geodesics on the surfaces. This leads naturally to the hypothesis that the visual system may estimate surface shape from texture flow by using a shape-from-contour mechanism: applying the differential equations for solving surface shape from contour derived in Section 3 to flow lines measured in oriented texture patterns.

The analysis of texture flow is organized into three subsections. Subsection 4.A develops the proposition that the flow lines of homogeneous, oriented textures follow geodesics of surfaces. Subsection 4.B discusses the particulars of solving shape from texture flow when applied to perfectly oriented textures (textures composed of strictly parallel line segments), to which the previous geometric analysis of contour information generalizes exactly. Finally, Subsection 4.C considers the problem of solving shape from texture flow for weakly oriented textures.

A. Texture Orientation, Homogeneity, and the Geodesic Constraint

The principal assumption on which all shape-from-texture models are based is that of homogeneity. The definition of statistical homogeneity of textures in the plane is straightforward. One would say that a texture

is nth-order homogeneous if its nth-order statistical correlations are translation invariant. This maps onto traditional notions of stationarity for stochastic processes; for example, a wide-sense-stationary process is one whose mean, variance and pairwise (second-order) correlations are translation invariant, while a strictly stationary process is one of which all the statistical moments are translation invariant.

Two of the properties assumed to be invariant with translation over a surface are the scale and "shape" of local texture. I will focus the current discussion on the latter class of assumptions. For textures in a plane, one can easily define homogeneity for all aspects of texture shape, including local compression and orientation of textures. Unfortunately, the extent to which we can generalize the concept of shape homogeneity to curved surfaces is limited. In order to include the concept of local texture orientation in the definition of shape, one requires a global concept of parallelism on a surface. This is possible only for developable surfaces; hence the ability to use gradients in local texture shape as a cue to surface shape in a consistent way is limited to textures projected from developable surfaces.

Developable surfaces are locally isometric to the plane; thus they can be unfolded, without stretching or compression, to a planar shape. This suggests a natural definition of homogeneity for textures on such surfaces: that the statistical properties of a texture are stationary in the 2D plane to which the surface unfolds. Let us represent a developable surface as a locally isometric mapping from the plane to 3D Euclidean space, $\Sigma = \mathbf{X}(u, v) : E^2 \rightarrow E^3$, where (u, v) are rectilinear coordinates in the plane. $\mathbf{X}$ can be thought of as characterizing the folding and twisting process that transforms the (u, v) plane into a developable surface in 3-space. We represent textures on a developable surface as samples of a 2D random field α, where $\alpha(u, v)$ is the texture "value" at a point (u, v) on a surface. α could characterize, for example, surface albedo, although we will assume for simplicity that it is scalar valued. The texture field on a developable surface is homogeneous if the texture field α is statistically stationary in the (u, v) plane.

We are concerned here with the information provided by the pattern of local texture orientations in an image (the texture flow); thus we require a definition of local surface-texture orientation. For present purposes, I assume a translation-invariant operator, ϕ, which, when applied to the texture field α gives a measure of local texture orientation in the (u, v) plane, $\theta(u, v) = \phi_{u,v}(\alpha)$. An example of such an operator is the orientation of the quadratic form derived from the second-order spatial moments of α (the orientations of locally fitted ellipses). Since ϕ is translation invariant and α is stationary, the resulting random orientation field θ is itself stationary.

The orientation field θ can be transformed into a random normal vector field $\mathbf{w}$ in the (u, v) plane, where

$$\mathbf{w}(u, v) = [\cos \theta(u, v), \sin \theta(u, v)]^T. \tag{20}$$

Since the (u, v) plane is isometrically mapped by X onto a developable surface Σ, the vector field $\mathbf{w}$ in the (u, v) plane is mapped to a 3D vector field $\mathbf{T}$ on the surface by $\mathbf{T}(u, v) = \partial X(u, v)[\mathbf{w}(u, v)]$, where ∂X is the differential of X, given by the matrix

$$\partial X = \left[\frac{\partial X}{\partial u} \frac{\partial X}{\partial v}\right] = \begin{bmatrix} \partial x/\partial u & \partial x/\partial v \\ \partial y/\partial u & \partial y/\partial v \\ \partial z/\partial u & \partial z/\partial v \end{bmatrix}. \tag{21}$$

I will refer to $\mathbf{T}$ as the texture flow field on a surface.

By definition, homogeneous textures in the plane are samples from a stationary stochastic process; therefore the mean vector field, $E[\mathbf{w}]$, computed over the entire ensemble of textures, is a constant. (In practice, homogeneity should also imply ergodicity; that is, that the spatial variation in local estimates of mean texture orientation will decrease with increases in the size of the window over which the estimates are computed.) For a given surface and a given texture ensemble, the mean flow field for textures mapped onto the surface is given by

$$E[\mathbf{T}(u, v)] = \partial X(u, v)[E[\mathbf{w}]]. \tag{22}$$

If we assume that the surface is smooth, then the mean texture flow field is a differentiable, unit-normal vector flow field. We can think of the mean flow field as a tangent vector field that can be integrated to derive a family of flow lines on the surface. Because the flow lines in the (u, v) plane are parallel straight lines and are mapped under an isometry to the surface, the flow lines on the surface are parallel geodesics; that is, the flow lines are parallel along rulings of the surface.[22] The situation is depicted in Fig. 10.

The geometric properties of homogeneous textures on developable surfaces suggest that we can apply the same method used to infer surface shape from parallel geodesic contours to infer surface shape from texture flow. Applying the method requires two stages: (1) estimating the projections of the mean texture flow lines, which would be equivalent to a set of parallel geodesic contours, and (2) integrating the geodesic-constraint equations along the flow lines to infer the underlying surface shape. In the following section I will consider a class of textures for which the first problem is trivial: perfectly oriented textures, composed of parallel sets of line segments. This simple case will illustrate the unique advantages offered by flow fields for the interpretation of surface shape. For most textures, however, the first problem is nontrivial, and Subsection 4.D will treat the geometric distortions in image texture flow fields composed of elements with some "width" (e.g., ellipses as opposed to idealized straight line or edge segments).

B. Estimating Shape from Texture Flow: Perfectly Oriented Textures

The projection equation mapping a straight line segment into the image is equivalent to the one mapping a curve's tangent to the tangent of its projected contour. Thus, assuming either orthographic or spherical perspective projection, the texture flow field in the image of a perfectly oriented texture is given by the 2D vector field,

$$\mathbf{t}(\theta, \omega) = \frac{[\mathbf{T}(\theta, \omega) \wedge \mathbf{V}(\theta, \omega)] \wedge \mathbf{V}(\theta, \omega)}{|\mathbf{T}(\theta, \omega) \wedge \mathbf{V}(\theta, \omega)|}, \tag{23}$$

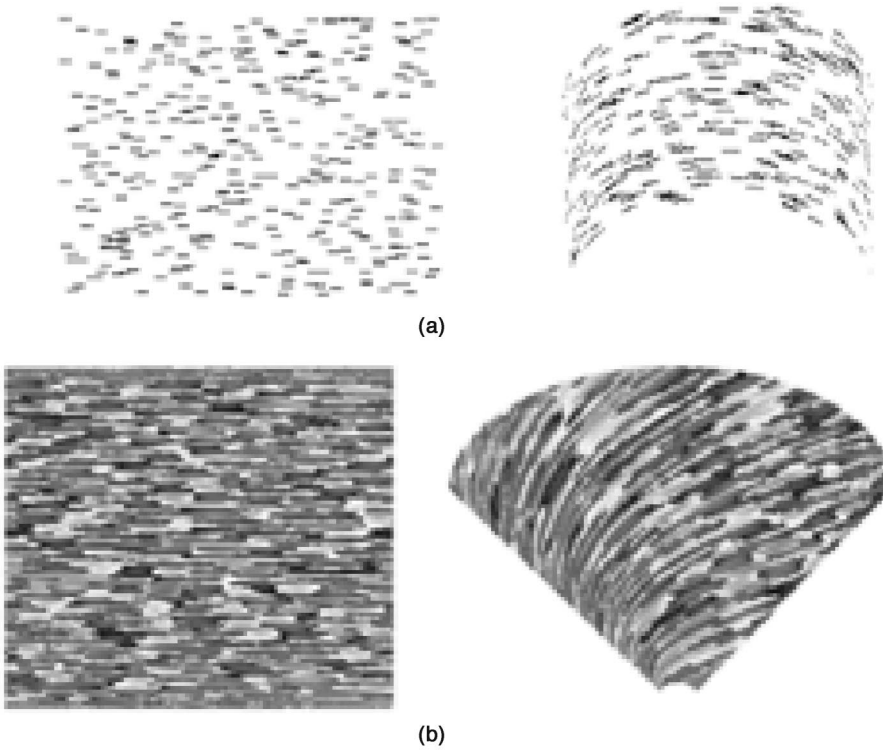

Fig. 10. (a) Oriented flow field composed of parallel line segments mapped under an isometry to parallel geodesics (in this case, lines of curvature) on a cylinder. (b) More natural oriented texture, mapped under an isometry to a cone. The apparent flow lines follow parallel geodesics of the cone.

where θ and ω are an arbitrary pair of parameters specifying position in the image, **T** is the texture flow field on the surface, and **V** is the viewing direction at the point (θ, ω) in the image. For orthography, **V** is constant. Treating **t** as a tangent field, one can integrate it to derive a family of imaginary contours (flow lines) whose geometry is equivalent to that of contours projected from parallel geodesics on a surface. This allows one to apply the differential equations [(14) for orthography or (16) and (19) for spherical perspective] to solving surface shape from texture flow.

A number of features of texture flow make estimating surface shape from texture flow notably simpler than estimating surface shape from geodesic contours. First, texture flow fields support direct estimation of the projected surface rulings even under spherical perspective, unlike pairs of surface contours. Since surface rulings project to great circles on the view sphere and the surface-texture flow field along surface rulings is parallel, the problem of finding the projected surface rulings reduces to that of finding the set of great circles along which the image texture flow **t** can be shown to be projected from a parallel field. Since parallel lines in the world project to great circles on the view sphere that intersect at a common pole of the sphere (see Fig. 11), projected rulings are characterized by the property that the great circles tangent to the texture flow along rulings intersect at a common pole. This property can be used to infer the projected rulings in a spherical image in much the same way as lines of parallelism are used in orthographic images. Second, since the texture flow field is a dense tangent field, one need not integrate the geodesic-constraint equation along a flow line but can do so along any curve in the image. This implies that occlusion is not the problem for texture flow that it is for contours. [Equation (19) is expressed in terms of arclength along a geodesic contour; thus integrating along a nonflow line, $\alpha(t)$, requires multiplying the left-hand side of the equation by a correction factor, $\partial s/\partial t$.]

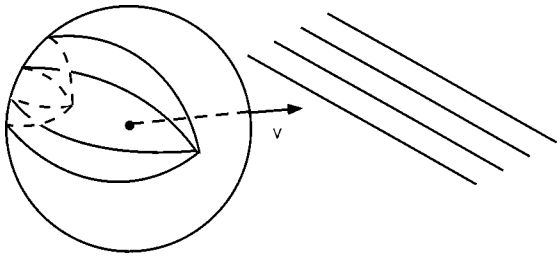

Fig. 11. Under spherical perspective, parallel lines in the world project to great circles on the view sphere that intersect at a common pole. Since the tangents of parallel texture flow lines along a surface ruling are parallel, their projections on the view sphere are tangent to great circles that intersect at a common pole.

C. Weakly Oriented Textures: Effects of Local Texture Shape

Perfectly oriented texture flows are clearly a strong source of information about the shape of a surface; however, few natural textures are perfectly oriented. The principal way in which most natural textures deviate from the idealized line-element model is that the local shape of textures has width as well as orientation. The prototypical example is a texture composed of ellipses,

which, while they might all be oriented in the same direction, have some nonzero aspect ratio. We will refer to such textures as weakly oriented textures. In general, the local orientation of a projected texture, as measured in the image, will not be equal to the projected orientation of the surface texture as defined by Eq. (23); hence the measured texture flow lines in the image will not equal the idealized projection of texture flow lines on the surface. In this section I analyze the errors in measured texture flow (measured as deviations from the idealized flow of perfectly oriented textures) for weakly oriented textures as a function of how strongly oriented the textures are (how closely the textures approach the thin-line-element model).

In order to treat the problem quantitatively, I will rely on a specific class of models for quantifying local texture orientation and shape: those based on local, second-order moments of a texture. Such models represent a texture field as a field of moment tensors, measured locally in a texture, each of which can be thought of as the quadratic form of an ellipse. An example of such a formulation, based on luminance gradient measures in an image is given below,

$$\mathbf{M}(x,y) = \begin{bmatrix} m_{xx}(x,y) & m_{xy}(x,y) \\ m_{xy}(x,y) & m_{yy}(x,y) \end{bmatrix} = \begin{bmatrix} \int\int_{\Omega_{(x,y)}} \frac{\partial^2 L(x,y)}{\partial x^2} & \int\int_{\Omega_{(x,y)}} \frac{\partial^2 L(x,y)}{\partial x \partial y} \\ \int\int_{\Omega_{(x,y)}} \frac{\partial^2 L(x,y)}{\partial x \partial y} & \int\int_{\Omega_{(x,y)}} \frac{\partial^2 L(x,y)}{\partial y^2} \end{bmatrix}, \tag{24}$$

where the integrals are computed over a small region of the image, $\Omega_{(x,y)}$, around a point. The formulation could easily be applied to characterizing local texture shape on a surface by replacing the luminance variable with an albedo variable. Other methods for computing such moment tensors exist, for example, measuring the statistical distribution of edge element orientations in a local region of texture[24,25] or measuring the second-order moments of the local spectrum of a texture.[26] All of the methods share the same geometric interpretation: Textures are represented as 2D fields of ellipses, defined by treating the local moment tensors as quadratic forms. A texture flow, then, is given by the vector field defined by local ellipse orientations. The strength of orientation of a surface texture is given by the aspect ratio of the average ellipse fitted to the local texture on a surface.

In the current analysis I will assume that one can define the local moments of the texture, α, on a surface in the same way as in the image. I will further assume that the measurement scale is small enough relative to the curvature of a surface and the viewing distance that we can approximate the local projection of a texture onto the view sphere as being orthographic along the line of sight. In this case the local image texture moment, $\mathbf{M}_I$, can be written as a function of the local surface texture moment, $\mathbf{M}_S$, as

$$\mathbf{M}_I = \mathbf{P}^{-1^T}\mathbf{M}_S\mathbf{P}^{-1}, \tag{25}$$

where $\mathbf{M}_S$ is computed in the (u, v) plane (the "unfolded" surface) and $\mathbf{P}$ is the differential of the map from the (u, v) plane into the image at the image position, (θ, ω) [the mapping from the (u, v) plane to the image is a composition of the mapping, X, from the (u, v) plane to the surface and the projective mapping into the image]. The image texture flow field is given by the vector field $\mathbf{t}$, defined by the normalized eigenvectors of $\mathbf{M}_I$ (with smallest eigenvalue), that is, the field of vectors oriented along the long axes of the ellipses defined by $\mathbf{M}_I$.

Figure 12 illustrates the problem presented by weakly oriented textures. It shows an oriented texture that has been mapped onto a Gaussian ridge and projected into the image. The aspect ratio of the local texture in this example is 0.5. Superimposed on the figure are the *projected* flow lines [the projections of the flow lines on the surface, computed with Eq. (23)] and the *image* flow lines (the flow lines of the vector field defined by the local texture moments of the image texture). Because the geodesic constraint equations characterize the relationship between the curvature of the projected flow lines and the curvature of the underlying surface, applying them to the image flow will lead to some error.

The difference between the image texture flow field and the projected flow field arises from the fact that the orientation vector of a projected ellipse is not equal to the projection of the orientation of the original ellipse, as illustrated in Fig. 13. Figure 13(a) shows three hypothetical elliptical texture elements on a surface along with the vectors specifying their orientations. Figure 13(b) shows the orthographic projections of the ellipses after the surface has been rotated away from the frontoparallel by 60° around the horizontal. Superimposed on the ellipses are pairs of vectors showing the projected orientation vectors and the orientation of the projected ellipses. Only the

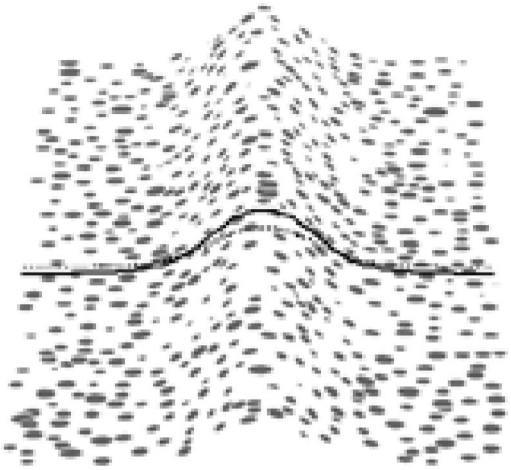

Fig. 12. Image of a texture composed of parallel ellipses with aspect ratio = 0.5, mapped onto a Gaussian ridge. The solid line represents the measured flow line in the center of the image, computed by integrating the flow field given by the set of ellipse orientations in the image. The dotted line represents the projected flow line in the center of the image, that is, the projection of a flow line on the surface. The projected flow line is not directly available to an observer. The difference between the measured flow line and the projected flow line reflects the error that would be induced in one's shape estimate should one apply the geodesic-constraint equation to the measured flow lines.

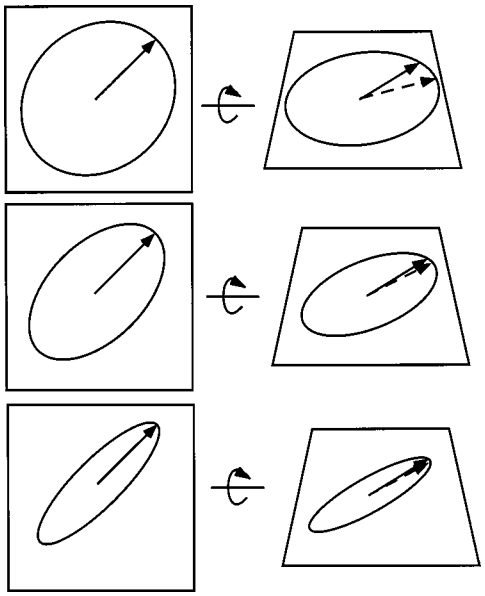

Fig. 13. Illustration of the effects of projection on ellipse orientation. Ellipses rotated out of the frontoparallel plane projected to ellipses in the image. The solid arrows on the left figures represent the orientation of the ellipses on the surface. The solid arrows on the right represent the projections of the orientation vectors, and the dashed arrows represent the orientations of the projected ellipses. The difference between the two illustrates the fundamental problem in directly applying the shape-from-contour theory to weakly oriented texture flows: The image texture flow as given by the texture-orientation field in the image deviates from the projection of the texture flow on the surface.

latter is available in the image. The difference between the two grows as the aspect ratio of the texture element approaches 1 (a circle).

In this section I set out to show, using selected calculations, that the problem posed to the model by weakly oriented textures is not as great as it might first appear; in particular, the difference between projected flow lines and image flow lines for weakly oriented textures is small for a large family of textures and for a large subset of viewing angles on a surface. I performed three sets of computer calculations. The first calculated the difference between the orientation of a projected ellipse and the projected orientation of the same ellipse as a function of the orientation of the surface on which the ellipse lies, the spin of the ellipse within that plane, and the aspect ratio of the ellipse. This measure quantifies the error in local orientation estimates induced by treating the image texture flow field as equivalent to the projected texture flow field. The second set of calculations computed a similar error in texture flow curvature for textures composed of dense fields of parallel ellipses. The final set of calculations was designed to evaluate the global effects of these local errors for image texture flows projected from cylinders and ridges.

The calculations characterize the difference between image texture flow (the vector field defined by local image texture orientation) and projected surface texture flow (the flow to which the contour equations apply). Because we were interested in the geometric distortion induced by the local shape of surface textures, we assumed for the calculations textures composed of dense, essentially continuous, fields of parallel ellipses. The errors described in the following sections, therefore, represent the error induced by treating image texture flow (assuming noiseless measures) as an estimate of the projected surface texture flow field. They do not include errors induced by problems with image measurements of texture flow, nor do they reflect the variability in image texture flow fields that would be induced by stochastic variation in local texture shape and orientation.

1. Orientation Error

The first calculations were designed to study the effects of projection on the local orientation of measured texture flow. To study these effects, I measured the difference between the projected orientation vector of an ellipse and the orientation of the projected ellipse as a function of the 3D pose of the ellipse in space (the slant of the underlying surface around the horizontal and the spin of the ellipse in the tangent plane of the surface: its orientation away from the horizontal axis). Some of these differences were illustrated in Fig. 13. Figure 14 shows the results for ellipses with aspect ratios of 0.125, 0.25 and 0.5. As expected, the error grows as the aspect ratio of the ellipse grows. Two other notable features of the results are that the error increases as the spin of the ellipse increases, that is, as the alignment of the ellipse approaches the tilt vector of the surface; and, similarly, it increases with increasing surface slant. These properties characterize the conditions in which the measured orientation of a weakly oriented texture flow will deviate from the idealized projected flow orientation.

2. Curvature Error

The second series of calculations was designed to study the effects of local texture shape on the curvature of the image texture flow field. The local curvature of a developable surface is characterized by the direction of maximal curvature in the tangent plane of the surface (orthogonal to the direction of the local surface ruling) and the value of the maximal curvature. The local curvature of the image texture flow is a function of five parameters: the slant of the surface, the direction and the quantity of maximal curvature of the surface, the direction of the flow on the surface relative to the direction of maximal curvature, and the aspect ratio of the texture on the surface. Since we are concerned with the proportional error in the curvature of measured texture flow (relative to the curvature of the projected flow lines), I explore only a four-dimensional parameter space in the calculations: the slant of the surface (arbitrarily fixing the tilt to be vertical), the direction of surface curvature relative to the tilt direction, the direction of texture flow relative to the direction of maximal curvature, and the aspect ratio of the flow.

Figures 15–17 show contour plots of proportional curvature error as a function of surface pose (surface slant and direction of maximal surface curvature). Surface slant is expressed in degrees away from the frontoparallel, the direction of surface curvature is given in degrees away from the horizontal (the surface is assumed to be slanted away in the vertical direction, i.e., about a horizontal axis), and the orientation of the texture flow (its

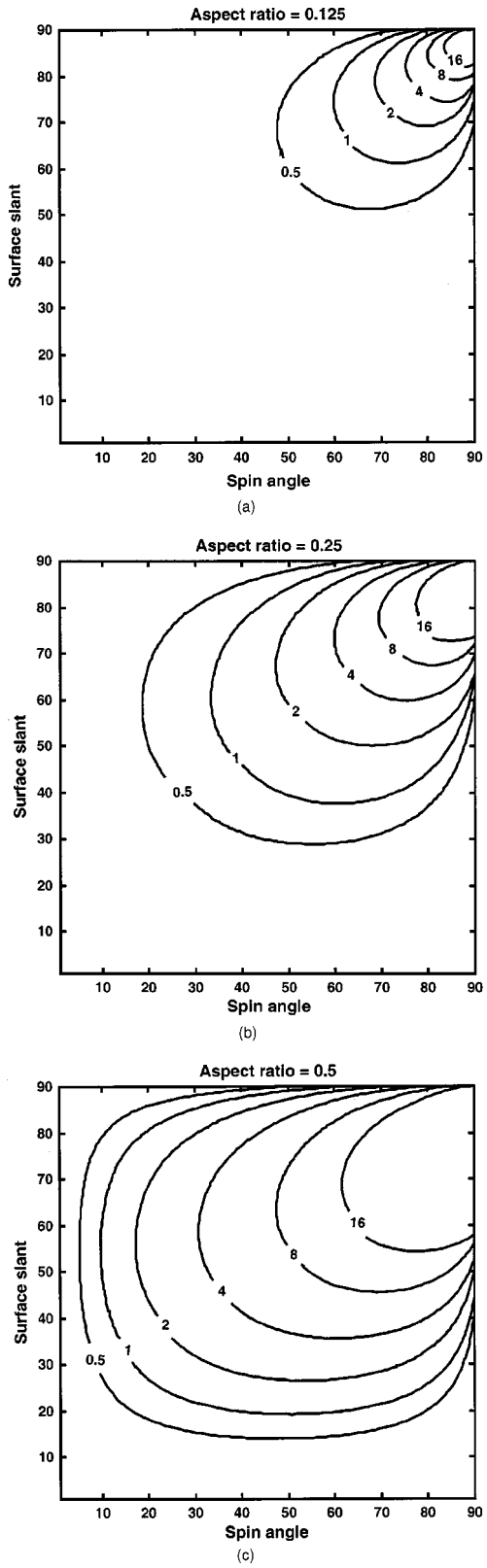

Fig. 14. Contour plot of the angular difference between the orientation vector of a projected ellipse and the projected orientation vector of an ellipse in the world. The error represents the orientation error induced by treating local image texture orientation as equivalent to the projection of the local orientation vector of a texture on a surface. Differences for textures with (a) an average aspect ratio = 0.125, (b) aspect ratio = 0.25, and (c) aspect ratio = 0.5.

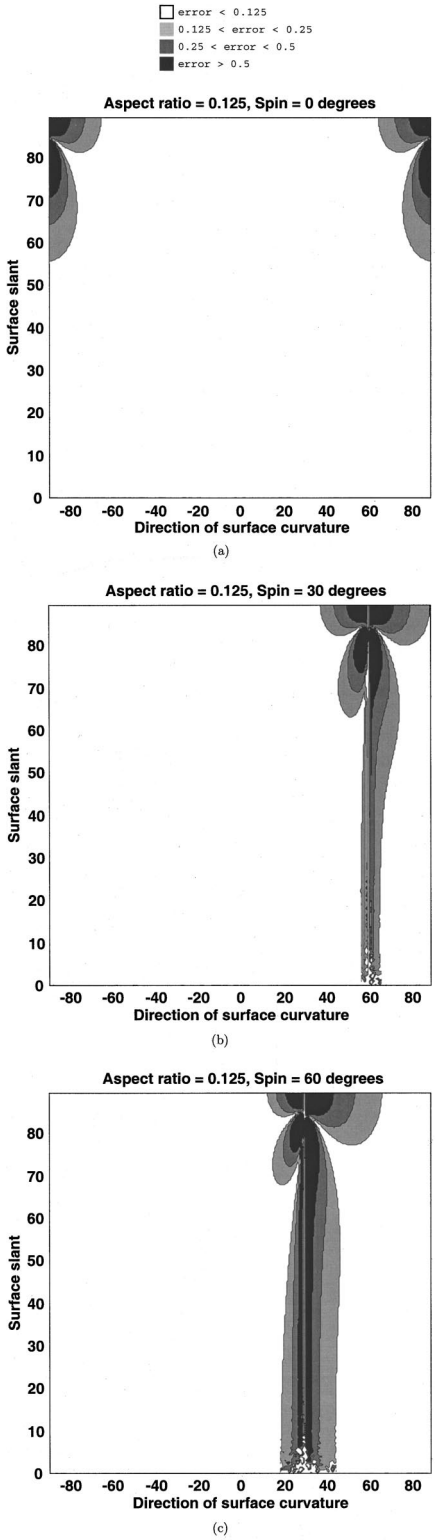

Fig. 15. Proportional difference between the curvature of the image texture-flow field and the true projected flow field for textures with three different orientations relative to the direction of maximal curvature: (a) 0° (flow is oriented along a line of curvature), (b) 30° (middle figure) and (c) 60°. The aspect ratio of the texture elements for the texture was fixed at 0.125. Proportional error is given by error = $|k_{\text{measured}} - k_{\text{projected}}|/k_{\text{projected}}$, where k_{measured} is the curvature of the image texture flow and $k_{\text{projected}}$ is the curvature of the projected surface texture flow field. Both slant and the direction of maximal surface curvature are given in degrees.

spin) is given in degrees away from the direction of maximal curvature. The orientation of the texture flow relative to the horizontal is given by the sum of the texture-flow spin and the direction of maximal surface curvature.

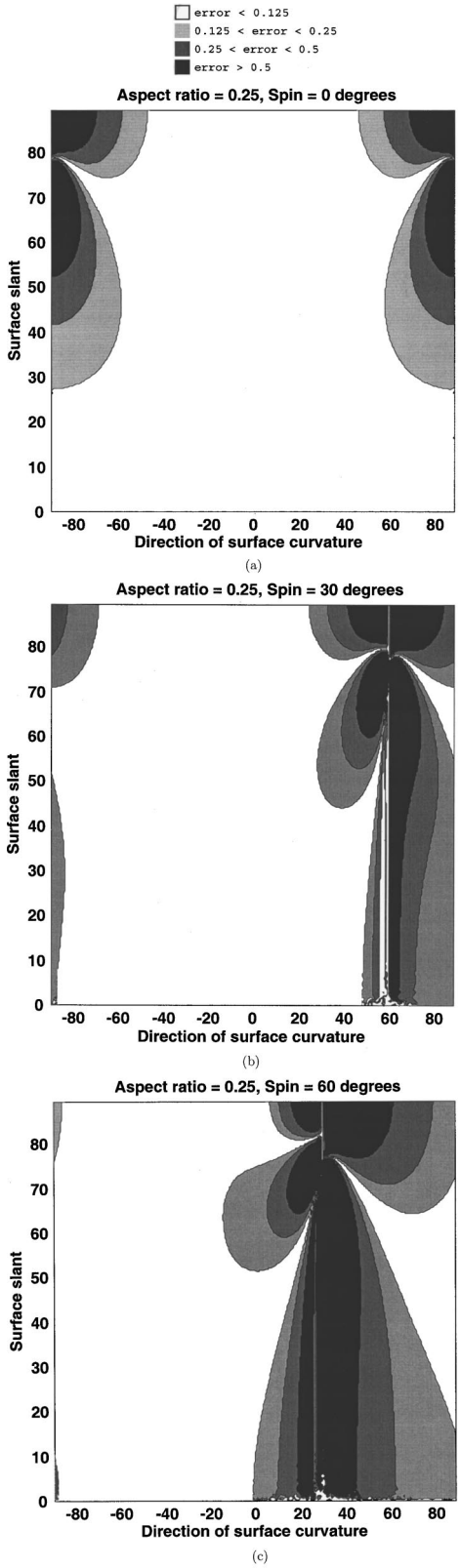

Fig. 16. Same as Fig. 15, but with a texture aspect ratio = 0.25.

The three figures correspond to different texture aspect ratios. For texture aspect ratios of 0.125 and 0.25, the range of surface poses for which the curvature error is below 25% is quite large. This low-error region shrinks as

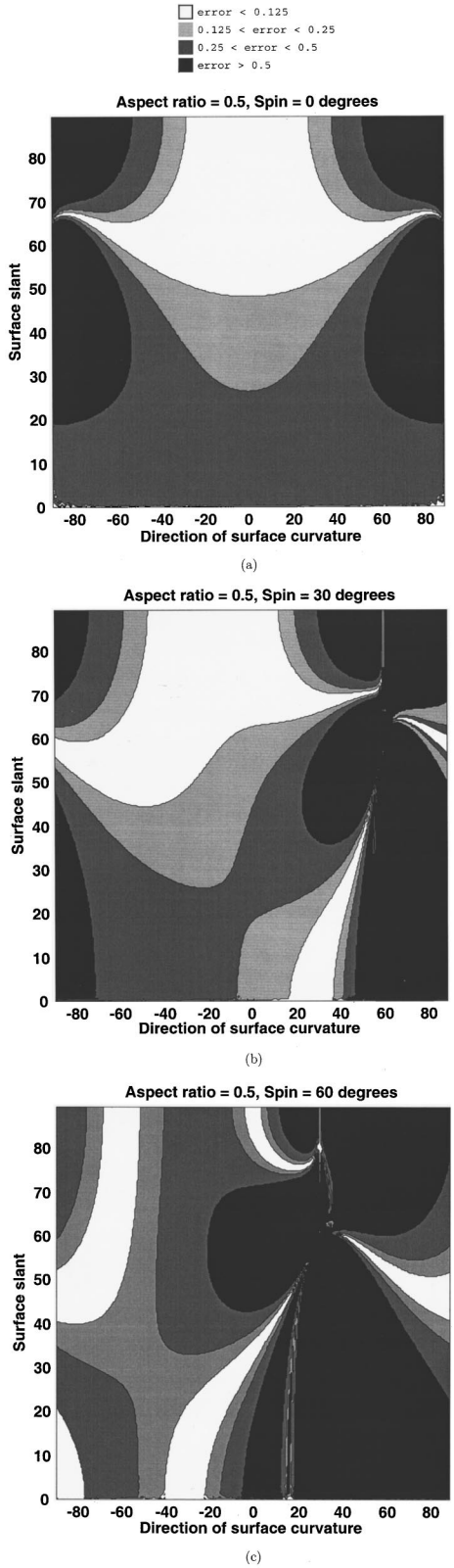

Fig. 17. Same as Fig. 15, but with a texture aspect ratio = 0.5.

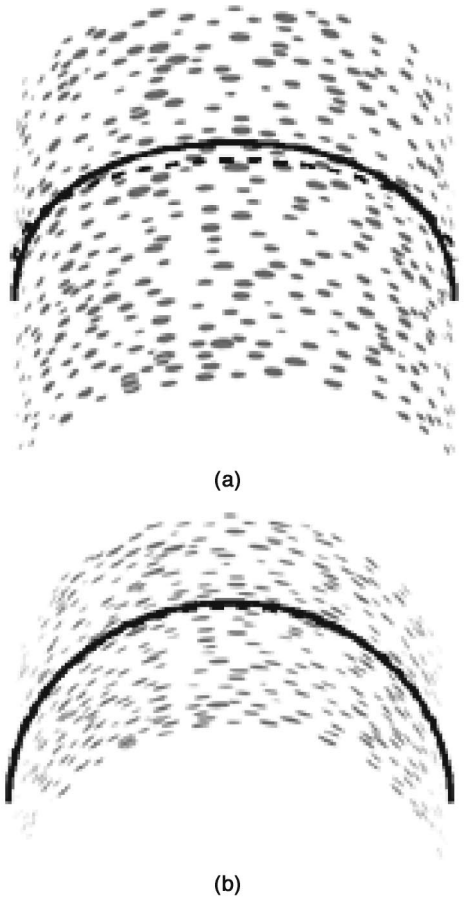

Fig. 18. Images of two texture fields of ellipses mapped onto cylinders oriented at (a) 30° and (b) 60° away from the frontoparallel plane. The texture field on the surface is composed of ellipses with an aspect ratio of 0.5, all oriented along the line of maximal curvature of the cylinder. The solid line shows the idealized image texture flow line through the center of the image (computed with a much denser array of ellipses than are shown in the figure), and the dashed line shows an idealized representation of the average projected texture-flow line. As described in the text, the image texture flow is computed from an orientation field derived from the ellipses in the image. The projected flow is computed by projecting the flow lines on the surface into the image. Only the former is directly available to an observer.

the aspect ratio increases. The plots for aspect ratios of 0.5 show large errors for a significant range of surface poses.

Note that the greatest proportional error is found when the texture flows in a direction aligned with the surface tilt, in this case, the vertical direction. Conversely, the proportional error tends to be low when the texture flows in the direction perpendicular to the surface tilt (the horizontal).

3. Global Texture Flow Errors

In order to evaluate the global impact of the local errors in image texture flow for weakly oriented textures, I calculated the image texture flow for dense fields of ellipses mapped onto cylinders for a number of different object poses in three dimensions. Image texture flow lines were computed by integrating the flow field estimated from the orientations of projected texture ellipses at each point in the image. Projected texture flow lines were computed by integrating the projection of the surface texture flow field from the center of the projected image to the self-occluding boundaries of the cylinder on either side.

Figure 18 shows flow lines computed for textures that follow lines of curvature on a cylinder. I have chosen to show only the image texture flow lines for textures whose aspect ratio is 0.5, as the deviation between projected flow lines and image flow lines decreases rapidly when the aspect ratio sinks below 0.5 (e.g., textures with an aspect ratio of 0.25 show little difference between projected and image flow lines). Figures 19 and 20 shows flow lines computed for textures oriented 30° away from the lines of curvature of the cylinder. For textures with an aspect ratio of 0.25, small difference appear in the projected and the measured flow lines. Even for textures with a large aspect ratio of 0.5 (very weakly oriented), however, the differences are small. Note further that the errors are greatest in regions of the image texture with the weakest

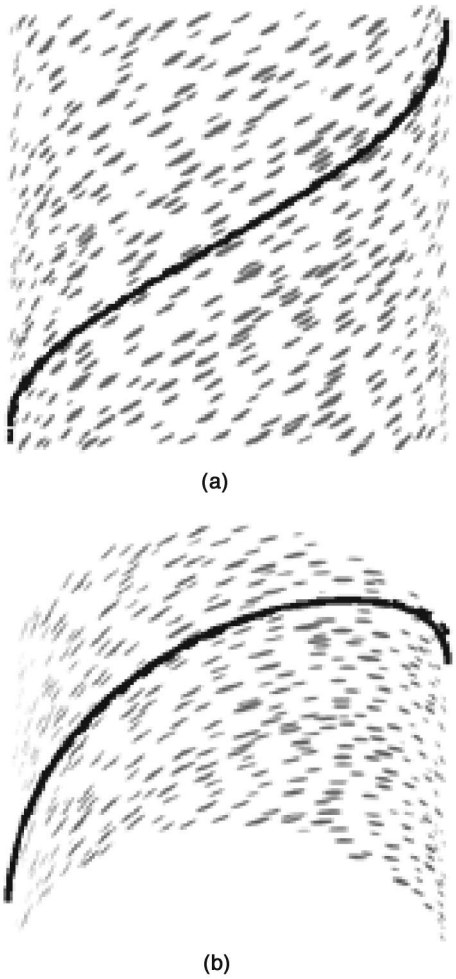

Fig. 19. Images of two texture fields of ellipses mapped onto cylinders oriented (a) in the frontoparallel plane and (b) 45° away from the frontoparallel plane. For both images the texture field contains ellipses with an aspect ratio = 0.25, all oriented at an angle of 30° away from the lines of maximal curvature of the cylinders. The solid line shows an idealized representation of the image texture flow line through the center of the image, and the dashed line shows an idealized representation of the average projected texture flow line.

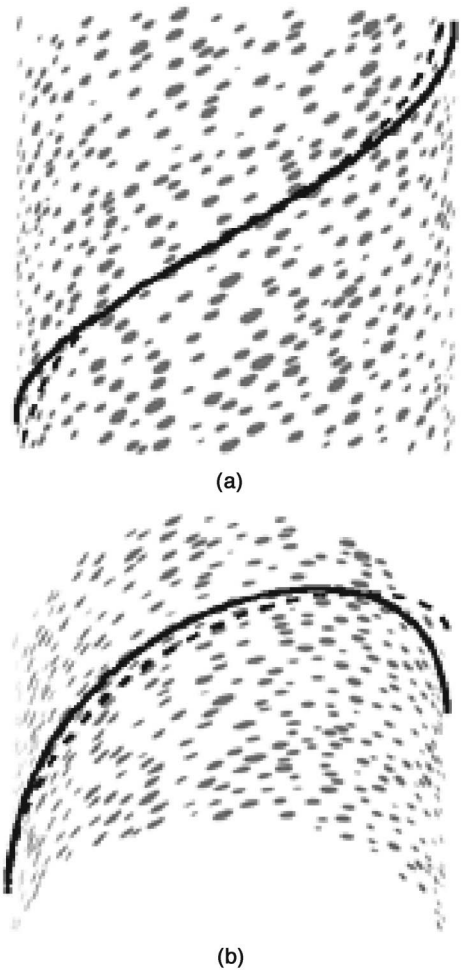

Fig. 20. Images of two texture fields of ellipses mapped onto cylinders oriented (a) in the frontoparallel plane and (b) 45° away from the frontoparallel plane. For both images the texture field contains ellipses with an aspect ratio = 0.5, all oriented at an angle of 30° away from the lines of maximal curvature of the cylinders. The solid line shows an idealized representation of the image texture flow line through the center of the image, and the dashed line shows an idealized representation of the average projected texture flow line.

orientation, that is, where the projected ellipses have the largest aspect ratios.

In the introduction to this section, I showed projected texture flow lines and image texture flow lines for a texture (aspect ratio = 0.5) on a Gaussian ridge surface (see Fig. 12). As with the previous simulations, the difference in curvature of the two flow lines reflects the error that would be induced by treating measured flow lines as equivalent to projected flow lines. The most notable feature about the figure, however, is that the qualitative shape of the flow lines remains invariant to the aspect ratio of the underlying texture. This is also true in the simulations shown here, suggesting that, while care must be taken in interpreting the absolute curvature of a surface from the flow lines in images of weakly oriented textures, one can reliably determine the qualitative shape of a surface from texture flow even for weakly oriented textures.

D. Conclusions

Homogeneous, oriented textures on developable surfaces flow along parallel geodesics of the surfaces. For textures that are strongly oriented (approximating parallel fields of straight line segments), therefore, the shape equations that apply to the estimation of surface shape from contour also apply to the flow lines in the images of such textures. These flow lines can be computed by integrating the measured orientation field in an image texture. Unlike the case of parallel contours imaged under perspective projection, texture flow fields support the direct estimation of projected surface rulings, an important step in simplifying the shape-estimation problem, a step that renders the problem one of simply integrating a first-order, nonlinear differential equation. Furthermore, the inherent noise in texture measurements can be significantly reduced by averaging the orientation field along lines of the projected rulings, resulting in a virtual contour that can be used as input to the integration process.

The major difficulty in applying the theory to real texture images is that most textures are composed of texture elements that have extended shapes (e.g., ellipses). The image texture flow field created by the projection of such textures is not equal to the projection of the texture flow field on the surface, as is required for strict validity of the geodesic-constraint equation. Numerical calculations, however, show that for a large range of object poses, the distortions between image texture flow fields and projected flow fields is small, even for textures whose average local aspect ratio is as large as 0.5. Furthermore, many manmade textures contain a small number of well-differentiated orientations (e.g., brick walls). These textures can be thought of as mixtures of strongly oriented textures. Mechanisms that segment a texture into its oriented components could serve as a first stage to a shape-from-texture flow process.

5. DISCUSSION

A. Evidence for Texture Flow Curvature As a Primary Shape Cue

Todd and Reichel[27] showed that textures composed of parallel, but disjoint, line segments on a curved surface could generate strong percepts of 3D shape similar to that generated by parallel lines mapped onto the same surface. In a more recent set of experiments, the current author measured the perceptual salience of textures as a function of their orientation strength.[28] Subjects viewed shaded and textured Gaussian ridges and were asked to localize the position of the ridge in the image. A perturbation technique was used to estimate the weights given by subjects to shading and texture in determining the perceived position of the ridge. Subjects gave approximately twice as much weight to texture when it was strongly oriented along the lines of curvature of the surface as when it was isotropic. Moreover, the weight given to texture increased monotonically with increasing texture orientation strength; that is, as the average aspect ratio of the texture elements decreased from 1 to 0.125.

Li and Zaidi[29] also found psychophysical evidence for the improved reliability of texture as a shape cue when it

is oriented along lines of curvature of a surface. They obtained measures of subjects' shape percepts for sinusoidal surfaces as depicted by textures containing, to varying degrees, strongly oriented components along the lines of curvature of the surface. They found that subjects' percepts of shape were much more accurate when textures contained a well-differentiated component that flowed along the lines of curvature of a surface than when it did not, including when the texture was perfectly isotropic. Subjects' estimates of the amplitude of the sine wave were greater, and they had fewer shape inversions (interpreting convex as concave, and vice versa), for the textures with good flow information. As in the current paper, Li and Zaidi suggested that the human visual system uses a shape-from-contour-like mechanism to interpret surface shape from texture flow, although they propose that the visual system incorporates Stevens' strong line of curvature constraint on the interpretation.

These studies suggest that textures that contain strongly oriented components along the lines of curvature of cylindrical surfaces provide optimal shape cues under many viewing conditions. By itself, this does not implicate a contour-like mechanism for the interpretation of shape from texture flow, as outlined in this paper. Any shape-from-texture model that accurately represents the texture homogeneity constraint (e.g., Malik and Rosenholtz's model of shape from local texture deformations[30]) might perform similarly; that is, the results may simply reflect the relative informativeness of different classes of textures, textures that flow along lines of surface curvature possibly being the most informative. It would be difficult to isolate the exact nature of the shape mechanism used to interpret shape from texture in the type of psychophysical experiment described above. I would, however, like to present one piece of indirect evidence in support of the theory that texture flow taps into a shape-from-contour-like mechanism in the human visual system. Figure 21 shows two images of a Gaussian ridge surface. The texture on one surface flows along lines of curvature of the surface, whereas on the other surface it flows along a direction 30° away from the line of curvature. The perceived shape of the second surface is clearly different from that of the first. It appears as a surface whose texture is, in fact, flowing along a line of curvature; that is, our visual systems seem to interpret the shape of the surface by using a strong bias to interpret the texture as flowing along lines of curvature of the surface.

The demonstration illustrates two important points about estimating surface shape from texture flow. First, one of of the principal ambiguities in the information provided by texture flow about surface shape is the direction of the texture flow relative to the lines of curvature on a surface. Estimation of the direction of the flow directly affects estimation of surface shape. Under orthographic projection, the ambiguity is absolute: a wide range of flow directions would be consistent with any given image of texture flow. In small fields of view, perspective contributes little to resolving this ambiguity. The second point illustrated by Fig. 21 is that the human visual system resolves the ambiguity by applying a prior bias to interpret flow as following lines of curvature on a surface, consistent with Li and Zaidi's proposal.[29] Such a bias fits naturally into a system designed to estimate shape from contour, but it has no natural implementation in a generic shape-from-texture model that simply measures local texture gradients, or deformations.

The preceding demonstration leads naturally to the question of whether the human visual system can interpret texture flow by using a generic geodesic constraint, as implied by homogeneity, or whether it necessarily applies the stricter line-of-curvature assumption. One answer to the question is that the line-of-curvature constraint is consistent with the homogeneity constraint only for cylindrical surfaces, for which the lines of curvature are also geodesics. Figure 3(b) shows a homogeneous, oriented texture on a cone. The flow in this figure does not follow lines of curvature of the surface. No homogeneous texture on a cone could follow lines of curvature, since lines of curvature on a cone are not geodesic. The same is true for any surface that is twisted in space. In such cases, the projected rulings indicated by the texture flow will not converge at a common point on the view sphere, thus providing reliable evidence that a surface is noncylindrcial.

Even if humans were able to distinguish between texture flows that follow lines of curvature and those which do not, one would have to question whether they are able to infer surface shape from texture flow when the flow did not follow lines of curvature. The demonstration in Fig. 22 suggests that humans can do this. The figure shows two cylindrical surfaces with texture flow in a direction 30° away from the line of maximal curvature of the surfaces. The surfaces appear, correctly, to be elongated toward the observer by different amounts, despite the fact that the shading on the two figures is the same. The difference in perceived shape is clearly attributable to the differences in texture flow, in this case, the smooth occluding contours of the surface constrain the interpretation of the surface to be convex, eliminating the line-of-

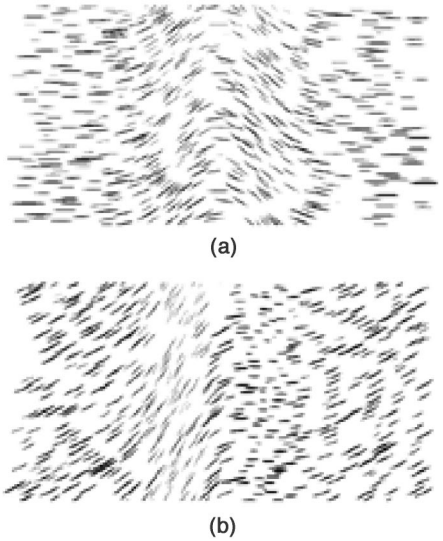

Fig. 21. Two oriented textures mapped onto a Gaussian ridge. (a) oriented along lines of maximal curvature on the surface, (b) oriented 37° away from the lines of maximal curvature. The shapes of the two surfaces appear markedly different. The texture in (b) appears to be interpreted as if the texture flowed along lines of curvature of a surface.

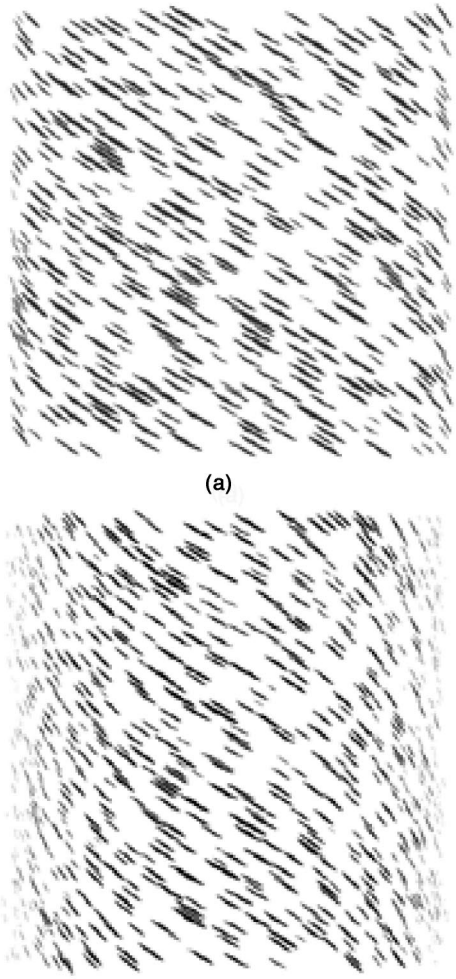

Fig. 22. Texture flow that does not follow lines of curvature on a cylindrical surface provides perceptually salient information about the curvature of the surface. (a) A homogeneous texture oriented 30° away from the line of maximal curvature on a flattened cylinder with aspect ratio = 0.66. (b) A similar texture pattern on an elongated cylinder with aspect ratio = 2.0. The surface in (b) clearly appears more elongated than the one on (a). In this case the virtual occluding contours on either side of the cylinder preclude a line-of-curvature interpretation for the texture.

curvature interpretation as a candidate estimate of surface shape. Thus the human visual system does appear to be able to estimate surface shape from texture flow without making recourse to the line-of-curvature constraint. It remains to be seen whether the salience of the cue is as strong in this case as it has been demonstrated to be when the texture flows along lines of maximal surface curvature.

B. Recovering Flow Lines

Having shown how texture flow can be used to infer surface shape and that human observers are sensitive to the information in texture flow, I would like to discuss briefly the problem of measuring texture flow. Several models have been proposed for doing this in the computational literature, though with an eye more toward texture classification than to shape estimation.[31] Psychophysical data from experiments directed at the question of contour completion also suggest the existence of mechanisms that would naturally support the estimation of average texture flow fields in an image. Most notable are results suggesting that facilitatory influences extend not only between aligned detectors[32,33] but also between detectors arranged in parallel with one another. Such facilitatory connections are exactly what would be required in a network designed to extract an average texture flow field from a noisy texture flow in an image.

C. Summary

I have derived a set of differential equations for the estimation of surface shape from a broad class of contours: those that project from geodesics on developable surfaces. These results apply naturally to the problem of estimating surface shape from homogeneous, oriented textures, as the homogeneity constraint implies that an oriented texture flows along geodesics of a developable surface. Although errors may be induced by applying the contour equations directly to the flow patterns estimated from weakly oriented texture patterns, simulations suggest that the errors will be small for a broad range of surface poses in three dimensions. Psychophysical evidence and a number of phenomenal demonstrations suggest that texture patterns that are strongly oriented (texture flow) generate more salient cues to surface shape than do textures that are isotropic. Moreover, texture flow may be a particularly effective cue to shape because it can tap into the same mechanisms in the visual system that are used to estimate surface shape from contour.

APPENDIX A

In this appendix I derive the equations relating contour curvature to surface-normal curvature for geodesic contours [Eq. (1) and (1) in the text]. The notation and variable definitions follow the conventions defined in Subsection 3.B of the paper.

1. Orthographic Projection

Under orthographic projection, the normal to a contour is related to the tangent direction of the 3D curve from which it projects by

$$\mathbf{n}(s) = \frac{\mathbf{T}(s) \wedge \mathbf{N}_S(s)}{|\mathbf{T}(s) \wedge \mathbf{N}_S(s)|}. \tag{A1}$$

The signed curvature of the contour is given by

$$\kappa(s) = \left\langle \frac{\partial \mathbf{n}(s)}{\partial s}, \mathbf{t}(s) \right\rangle, \tag{A2}$$

where $\mathbf{t}(s)$ is the tangent of the contour. Differentiating Eq. (A1), we obtain

$$\frac{\partial \mathbf{n}(s)}{\partial s} = \frac{\partial \mathbf{T}(s)/\partial s \wedge \mathbf{V}}{|\mathbf{T}(s) \wedge \mathbf{V}|} - \frac{\langle \partial T(s)/\partial s \wedge \mathbf{V}, \mathbf{T}(s) \wedge \mathbf{V}\rangle \mathbf{T}(s) \wedge \mathbf{V}}{|\mathbf{T}(s) \wedge \mathbf{V}|^3}, \quad \text{(A3)}$$

and substituting into Eq. (A2) gives for the signed curvature,

$$\kappa(s) = \frac{\langle \partial \mathbf{T}(s)/\partial s \wedge \mathbf{V}, \mathbf{t}(s)\rangle}{|\mathbf{T}(s) \wedge \mathbf{V}|} - \frac{\langle \partial \mathbf{T}(s)\partial s \wedge \mathbf{V}, \mathbf{T}(s) \wedge \mathbf{V}\rangle \langle \mathbf{T}(s) \wedge \mathbf{V}, \mathbf{t}(s)\rangle}{|\mathbf{T}(s) \wedge \mathbf{V}|^3}. \quad \text{(A4)}$$

$\mathbf{T}(s) \wedge \mathbf{V}$ is a vector in the image that is perpendicular to the tangent of the contour, so $\langle \mathbf{T}(s) \wedge \mathbf{V}, \mathbf{t}(s)\rangle = 0$ and Eq. (A4) simplifies to

$$\kappa(s) = \frac{\langle \partial \mathbf{T}(s)/\partial s \wedge \mathbf{V}, \mathbf{t}(s)\rangle}{|\mathbf{T}(s) \wedge \mathbf{V}|}. \quad \text{(A5)}$$

Because the 3D curve is a geodesic of a surface, $\partial \mathbf{T}(s')/\partial s'$, where s' is arc length along the 3D curve, is parallel to the normal vector of the surface and has a magnitude equal to the surface's normal curvature. We therefore have for $\partial \mathbf{T}(s)/\partial s$

$$\frac{\partial \mathbf{T}(s)}{\partial s} = \frac{\partial \mathbf{T}(s')}{\partial s'}\frac{\partial s'}{\partial s} = \kappa_{n_S}(s)\mathbf{N}_S(s)\frac{\partial s'}{\partial s}. \quad \text{(A6)}$$

Substituting into Eq. (A5) gives

$$\kappa(s) = \kappa_{n_S}\frac{\langle \mathbf{N}_S(s) \wedge \mathbf{V}, \mathbf{t}(s)\rangle}{|\mathbf{T}(s) \wedge \mathbf{V}|}\frac{\partial s'}{\partial s}. \quad \text{(A7)}$$

Using the backprojection equation

$$\mathbf{T}_S(s) = [\mathbf{t}(s) \wedge \mathbf{V}] \wedge \mathbf{N}_S(s)\frac{1}{|[\mathbf{t}(s) \wedge \mathbf{V}] \wedge \mathbf{N}_S(s)|}, \quad \text{(A8)}$$

$$\mathbf{T}_S(s) = \mathbf{n}(s) \wedge \mathbf{N}_S(s)\frac{1}{|\mathbf{n}(s) \wedge \mathbf{N}_S(s)|}, \quad \text{(A9)}$$

and substituting the expression derived in the text for $\partial s'/\partial s$, we have, finally,

$$\kappa(s) = \frac{\langle \mathbf{N}_S(s) \wedge \mathbf{V}(s), \mathbf{n}(s) \wedge \mathbf{V}(s)\rangle |\mathbf{n}(s) \wedge \mathbf{N}_S(s)|^2}{|[\mathbf{n}(s) \wedge \mathbf{N}_S(s)] \wedge \mathbf{V}(s)|\langle \mathbf{n}(s) \wedge \mathbf{V}(s), \mathbf{n}(s) \wedge \mathbf{N}_S(s)\rangle}\kappa_{n_S}(s). \quad \text{(A10)}$$

Inverting this, we obtain the expression given in the text for the surface-normal curvature,

$$\kappa_{n_S}(s) = \frac{|[\mathbf{n}(s) \wedge \mathbf{N}_S(s)] \wedge \mathbf{V}(s)|\langle \mathbf{n}(s) \wedge \mathbf{V}(s), \mathbf{n}(s) \wedge \mathbf{N}_S(s)\rangle}{\langle \mathbf{N}_S(s) \wedge \mathbf{V}(s), \mathbf{n}(s) \wedge \mathbf{V}(s)\rangle |\mathbf{n}(s) \wedge \mathbf{N}_S(s)|^2}\kappa(s). \quad \text{(A11)}$$

2. Spherical Perspective

Under spherical projection, the curvature of a contour is measured by its geodesic curvature on the view sphere. The contour itself is given by a curve, $\mathbf{x}(s)$, on the view sphere, and the viewing direction at any point on the contour is given by $\mathbf{V}(s) = -\mathbf{x}(s)$. The spherical analog to the normal along a contour in a planar image is the vector in the tangent plane of the spherical image that is perpendicular to the tangent of the contour,

$$\mathbf{w}(s) = \mathbf{t}(s) \wedge \mathbf{V}(s). \quad \text{(A12)}$$

The geodesic curvature of the contour is given by the projection of the contour's curvature vector onto the the tangent plane of the view sphere,

$$\kappa_g(s) = \left\langle \frac{\partial \mathbf{t}(s)}{\partial s}, \mathbf{w}(s)\right\rangle. \quad \text{(A13)}$$

It is straightforward to show that this is equivalent to

$$\kappa_g(s) = \left\langle \frac{\partial \mathbf{w}(s)}{\partial s}, \mathbf{t}(s)\right\rangle. \quad \text{(A14)}$$

Because spherical projection is locally orthographic, $\mathbf{w}(s)$ is related to the tangent of the 3D curve from which a contour projects by equation (A1)

$$\mathbf{w}(s) = \frac{\mathbf{T}(s) \wedge \mathbf{N}_S(s)}{|\mathbf{T}(s) \wedge \mathbf{N}_S(s)|}. \quad \text{(A15)}$$

Differentiating and substituting into equation (A14) gives for the geodesic curvature

$$\kappa_g(s) = \frac{\langle \partial \mathbf{T}(s)/\partial s \wedge \mathbf{V}(s), \mathbf{t}(s)\rangle}{|\mathbf{T}(s) \wedge \mathbf{V}(s)|} + \frac{\langle \mathbf{T}(s) \wedge \partial \mathbf{V}(s)/\partial s, \mathbf{t}(s)\rangle}{|\mathbf{T}(s) \wedge \mathbf{V}(s)|} - \frac{\langle \partial \mathbf{T}(s)/\partial s \wedge \mathbf{V} + \mathbf{T}(s) \wedge \partial \mathbf{V}(s)/\partial s, \mathbf{T}(s) \wedge \mathbf{V}\rangle \langle \mathbf{T}(s) \wedge \mathbf{V}, \mathbf{t}(s)\rangle}{|\mathbf{T}(s) \wedge \mathbf{V}|^3}. \quad \text{(A16)}$$

As before, the last term goes to zero. Also, because $\mathbf{V}(s) = -\mathbf{x}(s)$, $\partial \mathbf{V}(s)/\partial s = -\mathbf{t}(s)$ and the second term goes to zero, leaving

$$\kappa_g(s) = \frac{\left\langle \frac{\partial \mathbf{T}(s)}{\partial s} \wedge \mathbf{V}(s),\ \mathbf{t}(s) \right\rangle}{|\mathbf{T}(s) \wedge \mathbf{V}(s)|}. \quad \text{(A17)}$$

This is equivalent to equation (A5) for the orthographic case, and the remainder of the derivation is equivalent, with one exception, to that for orthographic projection. The only difference is in the expression for $\partial s'/\partial s$. In the case of perspective projection, this term must be multipled by a distance scaling factor, ρ, that is equal to the distance from the point in the world to the center of projection. The normal curvature of a surface viewed under spherical perspective is therefore related to contour curvature by Eq. (A11) with an added distance scaling term,

$$\kappa_{n_S}(s) = \frac{1}{\rho(s)} \frac{|[\mathbf{n}(s) \wedge \mathbf{N}_S(s)] \wedge \mathbf{V}(s)| \langle \mathbf{n}(s) \wedge \mathbf{V}(s),\ \mathbf{n}(s) \wedge \mathbf{N}_S(s) \rangle}{\langle \mathbf{N}_S(s) \wedge \mathbf{V}(s),\ \mathbf{n}(s) \wedge \mathbf{V}(s) \rangle |\mathbf{n}(s) \wedge \mathbf{N}_S(s)|^2} \kappa_g(s). \quad \text{(A18)}$$

ACKNOWLEDGMENTS

The author thanks Tjeerd Dijkstra for his help in the early stages of the project and for many helpful discussions during the development of the analysis. The research was completed in part while the author was an assistant professor in the Department of Psychology at the University of Pennsylvania. This research was funded by a grant from the National Institutes of Health, NIH-EY09383.

David Knill's e-mail address is knill@cvs.rochester.edu.

REFERENCES AND NOTES

1. J. J. Koenderink and A. J. van Doorn, "The shape of smooth objects and the way contours end," Perception **11**, 129–137 (1982).
2. J. J. Koenderink, "What does occluding contour tell us about solid shape," Perception **13**, 321–330 (1984).
3. D. A. Huffman, "Realizable configurations of lines in pictures of polyhedra," Mach. Intell. **8**, 493–509 (1971).
4. M. B. Clowes, "On seeing things," Artif. Intel. **2**, 79–116 (1971).
5. D. Waltz, "Understanding line drawings of scenes with shadows," in P. H. Winston, ed., *The Psychology of Computer Vision* (McGraw-Hill, New York, 1975), pp. 19–91.
6. V. S. Nalwa, "Line-drawing interpretation: a mathematical framework," Int. J. Comput. Vision **2**(2), 103–124 (1988).
7. F. Ulupinar and R. Nevatia, "Perception of 3-D surfaces from 2-D contours," IEEE Trans. Pattern Anal. Mach. Intell. **15**, 3–18 (1993).
8. S. A. Shafer and T. Kanade, "Using shadows in finding surface orientations," Comput. Vision Graph. Image Process. **22**, 145–176 (1983).
9. D. C. Knill, P. Mamassian, and D. Kersten, "The geometry of shadows," J. Opt. Soc. Am. A **14**, 3216–3232 (1997).
10. A. P. Witkin, "Recovering surface shape and orientation from texture," Artif. Intel. **17**, 17–47 (1981).
11. M. Brady and A. L. Yuille, "An extremum principle for shape from contour," IEEE Trans. Pattern Anal. Mach. Intell. **PAMI-6**, 288–301 (1984).
12. I. Weiss, "3D shape representation by contours," Comput. Vis. Graph. Image Process. **41**, 80–100 (1988).
13. T. Kanade, "Recovery of the three-dimensional shape of an object from a single view," Artif. Intel. **17**, 409–460 (1981).
14. K. A. Stevens, "The visual interpretation of surface contours," Artif. Intel. **17**, 47–73 (1981).
15. D. C. Knill, "Perception of surface contours and surface shape: from computation to psychophysics," J. Opt. Soc. Am. A **9**, 1449–1464 (1992).
16. R. Horaud and M. Brady, "On the geometric interpretation of image contours," Artif. Intel. **37**, 333–353 (1988).
17. F. Ulupinar and R. Nevatia, "Shape form contour—straight homogeneous generalized cylinders and constant cross-section generalized cylinders," IEEE Trans. Pattern Anal. Mach. Intell. **17**, 120–135 (1995).
18. P. Mamassian and M. S. Landy, "Observer biases in the 3D interpretation of line drawings," Vision Res. **38**, 2817–2832 (1998).
19. J. Wagemans, "Perceptual use of nonaccidental properties," Can. J. Psychol. **46**, 236–279 (1992).
20. M. P. Do Carmo, *Differential Geometry of Curves and Surfaces* (Prentice-Hall, Englewood Cliffs, N.J., 1976).
21. A. Jepson and W. Richards, "What makes a good feature?" in *Spatial Vision in Humans and Robots*, L. Harris and M. Jenkin, eds. (Cambridge U. Press, Cambridge, UK, 1992).
22. Garding[23] took a different tack to show that Rosenholtz and Malik's definition of homogeneity implies that surface texture orientations at neighboring points on a surface are equivalent under parallel transport. This result also implies that homogeneous, oriented textures flow along geodesics of developable surfaces.
23. J. Garding, "Surface orientation and curvature from differential texture distortion," presented at the 5th International Conference on Computer Vision, Cambridge, Mass., June 1995.
24. A. Blake and C. Marinos, "Shape from texture: estimation, isotropy and moments," *Oxford University Tech. Rep*. OUEL 1774/89 (Oxford U. Press, Oxford, UK, 1989).
25. J. Garding, "Shape from texture and contour by weak isotropy," Artif. Intel. **64**, 243–297 (1993).
26. B. Super and A. Bovik, "Shape from texture using local spectral moments," IEEE Trans. Pattern Anal. Mach. Intell. **17**, 333–343 (1995).
27. J. T. Todd and F. D. Reichel, "The visual perception of smoothly curved surfaces from double projected contour patterns," J. Exp. Psychol. **16**, 665–674 (1990).
28. D. C. Knill, "From contour to texture: static texture flow is a strong cue to surface shape," presented at the European Conference on Visual Perception, Helsinki, Finland, August 24–29, 1997.
29. A. Li and Q. Zaidi, "Shape from natural textures," Invest. Ophthalmol. Visual Sci. **40**, 2097 (1999).
30. J. Malik and R. Rosenholtz, "Recovering surface curvature and orientation from texture distortion: a least squares algorithm and sensitivity analysis," in *Proceedings of the 3rd European Conference on Computer Vision*, Vol. 800 of Lecture Notes in Computer Science (Springer-Verlag, Berlin, 1995), pp. 353–364.
31. A. R. Rao and R. C. Jain, "Computerized flow field analysis—oriented texture fields," IEEE Trans. Pattern Anal. Mach. Intell. **14**, 693–709 (1992).
32. Y. Bonneh and D. Sagi, "Effects of spatial configuration on contrast detection," Vision Res. **38**, 3541–3553 (1998).
33. M. Usher, Y. Bonneh, D. Sagi, and M. Herrmann, "Mechanisms for spatial integration in visual detection: a model based on lateral interactions," Spatial Vision **12**, 187–209 (1999).